Journal of Medicinal Chemistry

Clarkson.

Article

Preparation of Asymmetric Urea Derivatives that Target Prostate-Specific Membrane Antigen for SPECT Imaging

Naoya Harada, Hiroyuki Kimura, Masahiro Ono, and Hideo Saji

J. Med. Chem., **Just Accepted Manuscript** • DOI: 10.1021/jm400895s • Publication Date (Web): 24 Sep 2013

Journal of Medicinal Chemistry is published by the American Chemical Society. 1155 Sixteenth Street N.W., Washington, DC 20036

Preparation of Asymmetric Urea Derivatives that Target Prostate-Specific Membrane Antigen for SPECT Imaging

Naoya Harada, Hiroyuki Kimura, Masahiro Ono, Hideo Saji*

Department of Patho-Functional Bioanalysis, Graduate School of Pharmaceutical Sciences, Kyoto University, Kyoto, Japan

Abstract

Prostate-specific membrane antigen (PSMA) has been identified as a diagnostic and therapeutic target for prostate cancer.

(*S*)-2-[3-[(*R*)-1-carboxy-2-mercaptoethyl]ureido-pentanedioic acid (Cys-CO-Glu) were used to design novel PSMA targeting probes by nucleophilic conjugate addition between cysteine and maleimide based reagents.

3 ([^{123}I]IGLCE) was synthesized by this strategy and showed high affinity for PSMA. Results of binding inhibition assays of these derivatives suggested the importance of an aromatic group and succinimide moiety for high affinity. [^{123}I]**3** was evaluated *in vivo* with PSMA positive LNCaP and PSMA negative PC-3 human prostate cancer xenograft bearing mice. [^{125}I]**3** accumulated in LNCaP tumors but not in PC-3 tumors, and the accumulation was inhibited by 2-(phosphonomethyl)pentanedioic acid (2-PMPA). Use of [^{123}I]**3** provided positive images of LNCaP tumors in single photon emission tomography scans. These results warrant further evaluation of [^{123}I]**3** and its derivatives as radiolabeled probes for the diagnosis of prostate cancer.

Introduction

Prostate cancer is the most commonly diagnosed form of cancer and the second leading cause of cancer-related deaths among men worldwide.[1] Quantitation of concentrations of prostate specific antigen (PSA) concentrations, a serum tumor marker of prostate cancer, is effective for diagnosing prostate cancer.[2, 3] However, an invasive biopsy is required to confirm the diagnosis when the results of PSA tests are positive, because the PSA level is prone to elevation from other causes, such as aging and benign prostatic hyperplasia (BPH).[3, 4] Therefore, non-invasive diagnosis of prostate cancer using imaging techniques has significant clinical benefits.

Nuclear imaging techniques such as positron emission tomography (PET) and single photon emission computed tomography (SPECT) are valuable for noninvasive diagnosis. Currently, 2-deoxy-2-[^{18}F]fluoro-D-glucose ([^{18}F]FDG) is widely used as a PET probe for diagnoses of various cancers. However, [^{18}F]FDG is not suitable for diagnosis of prostate cancer because of the lack of correlation between [^{18}F]FDG uptake and tumor incidence.[5-8] Furthermore, [^{18}F]FDG uptake into the prostate of patients with BPH is similar to that of patients with prostate cancer.[5] Therefore, imaging probes that target prostate cancer-specific biomarkers are desired.

Prostate-specific membrane antigen (PSMA) is a useful target molecule for imaging and

radiotherapy of prostate cancer because of its high expression in this form of cancer and its transmembrane location.[9] PSMA is expressed in normal prostate, primary prostate cancer, and lymph node metastases of prostate cancer,[10] although PSMA expression in prostate cancer is 10–100-fold higher than expression in normal prostate tissue.[11] PSMA expression is up-regulated in patients with hormone-refractory prostate cancer, while PSA expression is decreased in the same patient population.[12] Because PSA is a secretory protein, metastases of prostate cancer cannot be diagnosed by the PSA test.[11] On the other hand, metastases can be diagnosed by PSMA imaging because PSMA is a membrane-anchored protein.[11]

^{111}In-labeled anti-PSMA monoclonal antibody [^{111}In]7E11-C5, marketed as ProstaScint, is a US Food and Drug Administration approved imaging agent for soft tissue metastases in patients with prostate cancer. It is not in widespread use, in part because it targets an intracellular epitope of PSMA and is believed to bind dead or dying prostate cancer cells.[13] More recently, ^{111}In-labeled monoclonal antibodies that bind to the extracellular domain of PSMA have been developed and shown to accumulate in prostate cancer xenograft bearing mice.[14] However, there have been limited clinical success using monoclonal antibodies because of their long circulating plasma half-life and low permeability in solid tumors, particularly for metastases to bone. Therefore, we believe that small molecule imaging agents should have a pharmacokinetic advantage.

PSMA has 86% sequence homology with glutamate carboxypeptidase-II (GCP-II).[9, 15, 16] Two structured pockets exist at the active site of GCP-II, which cleaves *N*-acetylaspartyl glutamate to *N*-acetyl aspartate.[17-19] Several asymmetric urea-based compounds (X-CO-Glu where X is an amino acid) are reported to be GCP-II inhibitors.[20] The glutamate moiety of urea-based inhibitors interacts with the S1′ pocket, while the other portions interact with the S1 pocket. Because there is a funnel-shaped tunnel with a depth of approximately 20 Å and width of 8–9 Å in the S1 pocket, urea-based compounds can be radio-labeled by introducing proper linkers to the amino acid residue without loss of affinity.[17, 21-26] Previously, PSMA probes with this motif have been reported, such as **23** ([^{123}I]DCIT)[27] and **24** ([^{123}I]MIP-1072)[28,29] (Figure 1). While [^{123}I]**23** had low affinity for PSMA and low tumor accumulation in LNCaP bearing mice, [^{123}I]**24** had high affinity for PSMA.[27, 28] Therefore [^{123}I]**24** appeares to be a promising probe for detection, prognosis, and monitoring prostate cancer, and further improvement of [^{123}I]**24** would be of benefit to clinical cancer research.[28, 29] However, [^{123}I]**24** is intolerant to modification because of its simple structure, which has proven difficult to improve by derivatization. In this study we aimed to find a new design strategy for asymmetric urea derivatives with high affinity to PSMA that were easy to design and modify.

Nucleophilic conjugate addition reactions between thiols and maleimides proceed under mild conditions. Utilizing this reaction, we have previously reported the synthesis of the

maleimide-based radio-iodination reagent, [^{123}I]**1** ([^{123}I]HML)[30] (Figure 2). [^{123}I]**1** can be easily prepared by iododestannylation, it rapidly reacts with thiols at room temperature, is stable in human serum, and is a peptidic reagent and thus derivatives are easily prepared by replacement of specific amino acids. **1** (Cys-CO-Glu), an asymmetric urea inhibitor of PSMA[31], has a reactive thiol (Figure 2). Therefore, using the reaction between **2** and derivatives of **1**, we can design and synthesize various types of PSMA probes. In this study, we prepared **3** ([^{123}I]IGLCE) via the nucleophilic conjugate addition reaction between **2** and [^{123}I]**1** (Figure 2).

The affinity of [^{125}I]**3** ([^{125}I]IGLCE) for PSMA was evaluated, and a rationale for its high affinity to PSMA was investigated. We hypothesized that the high affinity of [^{123}I]**3** for PSMA was attributable to interactions between the **1**-derived moiety and PSMA, and eight derivatives of **3** were designed (Figure 2). We focused on modifying the iodine, two amino acids (Lys and Gly), the aromatic ring, and the sccinimide in the **1**-derived moiety. The moieties important for high affinity were identified through a structure activity relationship study.

Additionally, the stability and biodistribution of [^{125}I]**3** was assessed, and SPECT/computed tomography (CT) imaging was performed to assess its utility.

RESULTS and DISCUSSION

Chemistry and Radiochemistry

As shown in Scheme 1, **3** was synthesized by a nucleophilic conjugate addition of the cysteine thiol of the asymmetric urea (**2**) with the maleimide moiety of **1**. The nonradioactive product, **3**, was analyzed by ^{1}H-NMR and FAB-HRMS. Its radiolabeled form, [^{123}I]**3**, was prepared from [^{123}I]**1**.[30] This labeling reaction proceeded under mild conditions (pH 6–8, room temperature) to afford high radiochemical yields (total yields were 58–63%). [^{123}I]**3** was prepared with a radiochemical purity greater than 95% after HPLC purification, and analysis of the purified [^{123}I]**3** showed a single peak (t_R: 23.1 min) corresponding to the isolated **3** (t_R: 23.0 min).

Eight derivatives of **3** were synthesized via the same conjugate addition approach (Schemes 2–4) and were employed to investigate the relationship between the structure of **3** and high affinity for PSMA. The appropriate active ester and maleimide-based ammonium **6a** or **6b** known in the literature[30] were condensed to yield the maleimide-based precursors **10a**, **10b**, **15a**–**15b**, **17**, and **21**. By only selecting the active ester, we could design these precursors. Introduction of several functional groups into the maleimide-based precursors was not difficult, such as the amino group of **21**. The methylamino group of active ester **20** was protected with

tert-butoxycarbonyl group but not with a benzyl group because maleimide was resistant to acid but not to hydrogenation. The condensation product of **20** and **6a** was deprotected with 4 N HCl/ethyl acetate to yield **21**. These maleimide-based precursors were reacted with **2** to yield the final products. All of these reactions proceeded at room temperature, and the final products were purified by reverse phase HPLC.

This synthetic strategy appears promising for the design of novel probes, not only for the derivatives that were synthesized, but also for PET probes, which generally have a short radiochemical half-life, as this reaction proceeds rapidly at room temperature.

***In Vitro* Cell-binding Assay**

Using Scatchard plots, the affinity of **3** for PSMA was evaluated by obtaining a K_d value using an *in vitro* cell-binding saturation assay. [^{125}I]**23** and [^{125}I]**24** were selected as positive control compounds to evaluate binding affinity.[27, 28] As shown in Table 1, [^{125}I]**3** had a higher affinity (K_d: 7.8 ± 1.4 nM) than [^{125}I]**23** (K_d: 143 ± 2 nM) and [^{125}I]**24** (K_d: 20.4 ± 0.6 nM).

We hypothesized that the high affinity of [^{123}I]**3** for PSMA was attributable to interactions between the **1**-derived moiety and PSMA. Eight derivatives (**11a**, **11b**, **16a**–**16c**, **18**, **19**, and **22**) of **3** were designed to further investigate the interactions between the **1**-derived moiety and PSMA and their affinities for PSMA were compared (Figure 2). The design of these

derivatives introduced four types of modifications into the **1**-derived moiety: substitution of the iodine for a proton (**11a**), substitution of a carboxyl group of Lys for a proton (**11b**), alteration of the carbon chain length of Gly (**16a**–**16c** and **18**), and removal of the iodobenzoyl group (aromatic group) (**19** and **22**). The affinities of these compounds for PSMA were evaluated in the binding inhibition assay.

The binding inhibition assay data are summarized in Table 2. Introduction of an iodine (**11a**) or carboxyl group (**11b**) into the **1**-derived moiety did not alter the affinity for PSMA. Alteration of the carbon chain length was acceptable since elongated (**16a**–**16c**) or shortened (**18**) carbon chain lengths of the **1**-derived moiety also did not affect the affinity. On the other hand, all of these derivatives, even **19**, which had a *N*-methylsuccinimidyl group appended to **2**, showed higher affinity (2.14–94.8 nM) than **2** (376 nM). This result suggested that the succinimidyl group of the **1**-derived moiety was important for high affinity. This finding supports the efficacy of the design strategy using **2** conjugated maleimide-based reagents.

Compounds **19** and **22** showed modest affinity (62.1–94.8 nM) compared with the other derivatives (2.14–8.06 nM). It appears that the aromatic group of the **1**-derived moiety was also important for high affinity because **19** and **22**, which did not have an aromatic group, had poorer affinity than the other derivatives (**3**, **11a**, **11b**, **16a**–**16c**, **18**), which had an aromatic group. These results suggested that both a succinimidyl group and aromatic group were

important for high affinity to PSMA although the distance between these moieties was not critical for the high affinity. We assessed this seemingly contradictory result using the X-ray structure of the binding site of PSMA, which had been reported by C. Barinka *et al*.[18, 19, 36, 37] In a previous report, C. Barinka *et al.* suggested that the glutamate moiety of urea-based inhibitors interacts with a pharmacophore (S1′ pocket), and the remainder of the inhibitor interacts with a lipophilic pocket (S1 pocket), which had been reported as a funnel-shaped tunnel with a depth of approximately 20 Å composed of hydrophobic β-sheets. Previously, M. Eder *et al.* had designed ^{68}Ga-labeled PSMA probes using the lipophilic chelator *N,N´*-bis[2-hydroxy-5-(carboxyethyl)-benzyl]ethylenediamine-*N,N´*-diacetic acid (HBED-CC) that targeted this hydrophobic pocket.[23, 38, 39] Applying the same logic to **3**, the **1**-derived moiety should interact with the S1 pocket, and the aromatic ring of the **1**-derived moiety should interact with the hydrophobic β-sheets of the S1 pocket. We also believe that the carbon chain length of **1** was not critical for high affinity because of the elongated structure of the hydrophobic S1 pocket.

To investigate these hypotheses, we performed a docking simulation study. The docking models between **3** and recombinant human GCP-II (rhGCP-II: PDB code 2c6c) are shown in Supporting Information. In these models, key interactions between the asymmetric urea moiety and the S1′ pocket were examined, including the cysteine moiety and Arg534, the urea group

and Gly518, and the glutamate moiety and Asn257, Lys699, and Try700 (Figure S1). These interactions corresponded with those identified in previous reports. In addition, interactions between the **1**-derived derived moiety and the S1 pocket were examined. As previously discussed, our results supported the importance of the succinimidyl and aromatic groups for achieving high binding affinity. In the docking simulation, the aromatic ring of the **1**-derived moiety was oriented to the hydrophobic S1 pocket, and the two oxygen atoms of the succinimidyl group interacted with Arg536 and Tyr549 (Figure S2). These interactions confirmed the importance of the aromatic and succinimidyl groups for obtaining high affinity.

***In Vitro* Stability**

We investigated the stability of [^{125}I]**3** using mouse serum. [^{123}I]**3** was expected to be stable since [^{123}I]**1** had been reported to be a stable radiolabeled reagent in human serum.[30] A portion of [^{125}I]**3** was degraded in mouse serum after an 18 h incubation period (Figure. 3B). This degradation product was probably *m*-[^{125}I]iodohuppric acid, which would be produced by cleavage of the Gly-Lys peptide bond. However, this degradation was not a rapid reaction, as no degradation products of [^{125}I]**3** were observed after a 6 h incubation period (Figures. 3A and 3B). In accordance with this result, [^{125}I]**3** was regarded as being stable. Indeed, long term stability would not be required since the majority of [^{125}I]**3** was excreted from blood 30 min

after injection in the subsequent biodistribution study.

Biodistribution and Blocking Studies

An *in vivo* biodistribution study of [^{125}I]**3** was performed using LNCaP- and PC-3-bearing mouse models to confirm the viability of our design strategy. The biodistribution data of [^{125}I]**3** and the tumor to blood or muscle ratios are shown in Table 3. [^{125}I]**3** showed good tumor uptake by LNCaP tumors (9.5% ID/g at 30 min), and this accumulation was maintained for at least 6 h, while low tumor uptake was observed in PC-3 tumors (0.94% ID/g at 30 min). Moreover, this high uptake in LNCaP tumors was significantly inhibited (0.55% ID/g at 30 min) by coinjection of 2-(phosphonomethyl)pentanedioic acid (2-PMPA) (50 mg/kg body weight) (Figure 4B). These results suggested that the tumor uptake of [^{125}I]**3** was due to PSMA-specific binding. Although high accumulation in the kidneys was also observed (89% ID/g at 30 min), the accumulation was inhibited (3.6%ID /g at 30 min) by coinjection of 2-PMPA (Figure 4A). GCP-II is expressed in mouse kidneys, which is likely responsible for the [^{125}I]**3** accumulation in this organ. Similar results have been observed with other probes targeting PSMA.[22, 23, 26, 27, 28, 31] [^{125}I]**3** also showed high accumulation in the spleen of C.B.-17/Icr *scid/scid* Jcl mice which was blocked with 2-PMPA indicating GCP-II expression in the spleen. [^{125}I]**3** showed fast blood clearance (8.9% ID/g at 2 min and 1.5% ID/g at 30 min,

respectively) and rapid pharmacokinetics as both the tumor/blood and tumor/muscle ratios reached high values after only 30 min (5.3 and 11.1, respectively). [^{125}I]**3** showed little deiodination as accumulation of radioactivity in the thyroid was not observed. These results suggested the possibility of the use of [^{125}I]**3** as a PSMA targeted probe that possesses good accumulation in PSMA-expressing prostate cancer tissue with rapid pharmacokinetics, and high stability.

In addition to [^{125}I]**3**, we prepared [^{125}I]**11b** and evaluated it *in vivo* (its radiosynthesis is shown in Supporting Information). [^{125}I]**11b** showed more rapid clearance from blood and slightly lower accumulation in LNCaP tumor than [^{125}I]**3** (Figure S4). However, [^{125}I]**11b** showed significantly higher accumulation in liver and intestine than [^{125}I]**3** (Figure S3). We considered that such high hepatic and intestinal accumulations of [^{125}I]**11b** were not preferable, and we attributed this accumulation to the lower polarity of [^{125}I]**11b** compared with that of [^{125}I]**3** (Table S1). This was supported by the fact that [^{125}I]**11b** had a longer HPLC retention time indicating it was lower in polarity than [^{125}I]**3**. Moreover, other iodinated derivatives (**16a**–**16c** and **18**) also had longer HPLC retention times than [^{125}I]**3** (Table S1). Therefore, we regarded [^{123}I]**3** as the best of the tested derivatives.

Then using mice, we compared the properties [^{125}I]**3** with the previously reported PSMA probe [^{125}I]**24**, for which a phase I clinical trial was completed. In accordance with the

previous study, high accumulation of [^{125}I]**24** in LNCaP tumor was observed (Table S2). [^{125}I]**24** showed higher accumulation in LNCaP tumor and kidney than [^{125}I]**3**, although the affinity of [^{125}I]**24** for PSMA was lower than [^{125}I]**3**. We consider that rapid clearance of [^{125}I]**3** from blood is the cause of this lower accumulation. [^{125}I]**3** showed lower radioactivity than [^{125}I]**24** in blood 30 min after injection. The differences in blood clearance may be attributed to differences in the excretion routes. [^{125}I]**3** was excreted from both kidney and liver. [^{125}I]**3** showed high accumulation in kidney, and accumulation in intestine was elevated over time. On the other hand, [^{125}I]**24** was excreted from kidney but not from liver. The lower hydrophilicity of [^{125}I]**11b** compared to [^{125}I]**3** is likely the cause of its higher hepatic accumulation of [^{125}I]**11b**. We also believed that lower hydrophilicity is likely the cause of the higher hepatic accumulation of [^{125}I]**3** compared to [^{125}I]**24**. The distribution coefficient (log D) of [^{125}I]**3** and [^{125}I]**24** is shown in Table S3. [^{125}I]**3** had a larger log D value (log D = -1.97) than [^{125}I]**24** (log D = -2.91). Therefore, an improvement of the hydrophilicity would be necessary for lowering hepatic accumulation and elevating tumor accumulation.

Small Animal SPECT/CT

A SPECT/CT study was performed on the basis of the biodistribution study results. SPECT scanning commenced 30 min after injection of [^{123}I]**3** since the tumor/blood ratio was

sufficiently high at this time point to obtain SPECT images. Although the tumor/blood ratio was higher 3 h after injection, the 30 min delay was selected as the time point for SPECT scanning in order to determine whether [^{123}I]**3** could distinguish LNCaP tumors from PC-3 tumors immediately after injection.

[^{123}I]**3** clearly distinguished LNCaP tumors from PC-3 tumors on SPECT/CT images 30 min post injection (Figures. 5A and 5C), and tracer accumulation was clearly absent from SPECT images when coinjected with 2-PMPA (Figure 5B). These results were consistent with those from the biodistribution study, and suggested that [^{123}I]**3** would be efficient as a PSMA targeting probe.

CONCLUSION

The syntheses of PSMA targeting derivatives by a nucleophilic conjugate addition between the cysteine of the asymmetric urea compound (**2**) and a maleimide based reagent were successful, and the aromatic and succinimidyl moieties of these derivatives were found to be important for high affinity. [^{123}I]**3**, which was synthesized by this reaction, exhibited high affinity for PSMA and gave clear SPECT images with LNCaP bearing mice.

This study clearly established the basis of a new design strategy for PSMA probes. Through our investigation of [^{125}I]**3**, we clarified the importance of the aromatic ring and the succinimidyl group for high affinity. Moreover, the significance of hydrophilicity for pharmacokinetics was confirmed.

These findings warrant further evaluation of [^{123}I]**3** as an imaging agent, and support the benefit of this strategy for design of other PSMA probes.

EXPERIMENTAL SECTION

General

W-Prep 2XY (Yamazen Corporation, Osaka, Japan) was used for silica gel column chromatography on a Hi Flash™ silica gel column (40 mm, 60 Å, Yamazen). Silica gel 60 F254, 0.5 mm (Merck KGaA, Darmstadt, Germany) was used for preparative thin layer chromatography (PTLC). A LC-20AD (SHIMADZU CORPORATION, Kyoto, Japan) equipped with a SPD-20A UV detector (ρ; 220 nm and 254 nm) (SHIMADZU) and a NDW-351 radioisotope detector (Hitachi Aloka Medical, Ltd., Tokyo, Japan) was used for high performance liquid chromatography (HPLC). The eluent consisted of a binary mixture of 0.1% trifluoroacetic acid (TFA) in H_2O (solvent A) and 0.1% TFA in methanol (solvent B). Nanopure water was prepared by MQ Integra15 (Nihon Millipore, Tokyo, Japan). Mass spectra were recorded on a LCMS-2010 EV (SHIMADZU), GCMS-QP2010 Plus (SHIMADZU), or JMS-SX 102A QQ (JEOL Ltd., Tokyo, Japan). ^{1}H-NMR spectra were recorded on a LNM-AL500 (JEOL) using $CDCl_3$, dimethylsulfoxide-*d*6 (DMSO-*d*6), CD_3OD, or D_2O as the solvent and tetramethylsilane as an internal standard (Euriso-top, Saint-Aubin, France). All chemicals used in the syntheses were reagent grade.

Chemistry and Radiochemistry

2 was synthesized as previously reported.[31] **1**,[30] **23**,[27] **24**,[28, 32] and radioiodinated forms of these compounds were synthesized by previously reported methods. [^{123}I]**3** was prepared by incubation of **2** with [^{123}I]**1** at room temperature for 15 min. Each radiolabeled compound was purified by reverse-phase HPLC using a COSMOSIL 5C_{18}-AR-II 4.6 × 150 mm column eluted with 0.1% TFA in water (solvent A) and 0.1% TFA in methanol (solvent B). An HPLC gradient with a flow rate of 1 mL/min was initiated from an isocratic system (30% solvent B) over 10 min and adjusted to 30–60% solvent B over 10 min followed by 60% solvent B.

Compounds **11a**, **11b**, **16a**–**16c**, **18**, **19,** and **22** were synthesized to investigate the relationships between the high affinity of **3** and its structure (Schemes 2–4). Compounds **4**–**6**,[30] **9a**,[30] **10a**,[30] **12**,[33] and **20**[34] were synthesized by previously reported methods. All compounds tested in the inhibition assay were prepared in > 95% purity as judged by HPLC. Conditions for HPLC purification are defined as follows: condition 1, YMC-Pack ODS-AQ 20 × 250 mm column (YMC Co. Ltd., Kyoto, Japan), 5 mL/min, 30–80% gradient of solvent B over 60 min; condition 2, YMC-Pack ODS 20 × 250 mm column, 5 mL/min, 40–90% gradient of solvent B over 60 min.

(2*S*)-2-(3-((1*R*)-1-Carboxy-2-((1-((*R*)-5-carboxy-5-(2-(3-iodobenzamido)acetamido)pentyl)-2,5-dioxopyrrolidin-3-yl)thio)ethyl)ureido)pentanedioic acid (3)

To a solution of **2** (6.8 mg, 0.023 mmol) in H_2O (0.2 mL) was added **1** (11.9 mg, 0.023 mmol) in acetonitrile (0.15 mL). 2 N NaOH was added to the mixture to adjust the pH to 7. The mixture was stirred at room temperature for 2 h. HPLC purification afforded **3** (3.8 mg, 21% yield) under the following conditions: COSMOSIL $5C_{18}$-AR-II column (10 × 250 mm) eluted with 0.1% TFA in water (solvent A) and 0.1% TFA in methanol (solvent B), at a flow rate of 2 mL/min, and an HPLC gradient initiated from an isocratic system (30% solvent B) over 15 min, adjusted to 30–60% of solvent B over 10 min followed by 60% of solvent B. ^{1}H-NMR (500 MHz, D_2O) δ; 8.10 (s, 1H), 7.90 (d, *J* = 8.02 Hz, 1H), 7.71 (d, *J* = 7.45 Hz, 1H), 7.21 (dd, *J* = 7.45, 8.02 Hz, 1H), 4.39 (t, *J* = 5.73 Hz, 1H), 4.28 (broad s, 1H), 4.15 (m, 1H), 3.99–4.07 (m, 2H), 3.93 (m, 1H), 3.39 (t, *J* = 6.87 Hz, 2H), 2.95–3.35 (m, 3H), 2.56 (m, 1H), 2.38 (dt, *J* = 2.86, 7.45 Hz, 2H), 2.05 (m, 1H), 1.83 (m, 2H), 1.65 (m, 1H), 1.48 (m, 2H) and 1.21 (t, *J* = 7.45 Hz, 2H). ESI-MS; 808 $[M + H]^+$. HRFAB$^+$-MS: calcd for $C_{28}H_{35}N_5O_{13}SI$, 808.0994 $[M+H]^+$; found 808.0997.

4-Methoxybenzyl 2-(3-iodobenzamido)acetate (7a)

To a solution of 3-iodobenzoic acid (2.8 g, 11 mmol) in *N*,*N*-dimethylformamide (DMF) (25 mL) was added 4-methoxybenzyl 2-aminoacetate hydrochloride (H-Gly-OPMB· HCl) (2.6 g, 11 mmol), water soluble carbodiimide hydrochloride (WSCI· HCl) (2.1 g, 11 mmol), and

triethylamine (1.1 mL). The mixture was stirred at room temperature for 6 h. After extraction with ethyl acetate, the organic layer was washed with brine and dried over sodium sulfate. The solvent was removed under reduced pressure, and the product **7a** was purified by silica gel column chromatography (hexane/ethyl acetate = 2/1, 3.0 g, 64% yield). ^{1}H-NMR (DMSO-*d*6): 9.06 (m, 1H), 8.20 (m, 1H), 7.92 (m, *1*H), 7.87 (m, 1H) 7.31 (m, 2H), 6.93 (m, 2H), 5.08 (s, 2H), 4.03 (d, J = 5.73 Hz, 2H), and 3.75 (s, 3H). EI-MS *m/z*: 425 $[M]^+$, 231 (4.7), 121 (100).

4-Methoxybenzyl 2-benzamidoacetate (7b)

To a solution of benzoic acid (1.6 g, 13 mmol) in DMF (15 mL) was added H-Gly-OPMB· HCl (3.0 g, 13 mmol), WSCI· HCl (2.5 g, 13 mmol), and triethylamine (1.8 mL). The mixture was stirred at room temperature overnight. After extraction with ethyl acetate, the organic layer was washed with brine and dried over sodium sulfate. The solvent was removed under reduced pressure, and the product **7b** was purified by silica gel column chromatography (hexane/ethyl acetate = 2/1, 2.2 g, 57% yield). ^{1}H-NMR ($CDCl_3$): 7.81 (d, J = 7.45 Hz, 2H), 7.51 (m, 2H), 7.45 (t, J = 7.45 Hz, 2H), 7.32 (m, 2H), 6.90 (m, 2H), 6.63 (s, 1H), 5.17 (s, 2H), 4.26 (d, J = 4.58 Hz, 2H), and 3.82 (s, 3H). EI-MS *m/z*: 299 $[M]^+$, 162 (2.0), 137 (4.7), 134 (15.9), 121 (100), 77 (34.7).

2-(3-Iodobenzamido)acetic acid (8a)

To a solution of **7a** (3.0 g, 7.1 mmol) in dichloromethane (24 mL) was added TFA (5.3 mL). The mixture was stirred at room temperature for 15 min. The solvent was removed under reduced pressure, and the product **8a** was recrystallized from chloroform (2.1 g, 97% yield). ^{1}H-NMR (CD_3OD) δ: 8.95 (m, 1H), 8.22 (t, J = 1.72 Hz, 1H), 7.92 (m, 1H), 7.88 (m, 1H), 7.30 (t, J = 8.02 Hz, 1H), and 3.92 (d, J = 5.73 Hz, 2H). ESI-MS *m/z*: 304 $[M]^-$.

2-Benzamidoacetic acid (8b)

To a solution of **7b** (2.2 g, 7.3 mmol) in dichloromethane (25 mL) was added TFA (5.5 mL). The mixture was stirred at room temperature for 15 min. The solvent was removed under reduced pressure, and the product **8b** was recrystallized from chloroform (1.2 g, 94% yield). ^{1}H-NMR (DMSO-*d*6) δ: 8.81 (t, J = 5.73 Hz, 1H), 7.87 (m, 2H), 7.55 (m, 1H), 7.48 (t, J = 7.45 Hz, 2H), and 3.93 (d, J = 5.73 Hz, 2H). EI-MS *m/z*: 179 $[M]^+$, 134 (20), 105 (100), 77 (69).

2,5-Dioxopyrrolidin-1-yl 2-benzamidoacetate (9b)

To a solution of **8b** (1.2 g, 6.7 mmol) in DMF (10 mL) was added *N*-hydroxysuccinimide (NHS) (0.78 g, 6.8 mmol) and *N*,*N*'-diisopropylcarbodiimide (DIC) (0.86 mg, 6.8 mmol). The mixture was stirred at room temperature for 14 h. After extraction with ethyl acetate, the

organic layer was washed with brine and dried over sodium sulfate. The solvent was removed under reduced pressure, and the resulting white precipitate was washed with chloroform and collected (1.8 g, 95% yield). ^{1}H-NMR (DMSO-*d*6) δ: 9.16 (t, *J* = 5.73 Hz, 1H), 7.88 (d, *J* = 7.45 Hz, 2H), 7.58 (t, *J* = 6.87 Hz, 1H), 7.50 (t, *J* = 7.73 Hz, 2H), 4.43 (d, *J* = 5.73 Hz, 2H), 2.82 (s, 4H).

(*S*)-2-(2-Benzamidoacetamido)-6-(2,5-dioxo-2,5-dihydro-1*H*-pyrrol-1-yl)hexanoic acid (10a)

To a solution of **9b** (0.1 g, 0.36 mmol) in acetonitrile (3 mL) was added **6a** (95 mg, 0.36 mmol) and *N,N*-diisopropylethylamine (DIPEA) (0.13 mL). The mixture was stirred at room temperature for 3 h. After extraction with ethyl acetate and washing with saturated aqueous ammonium chloride, the organic layer was dried over sodium sulfate. The solvent was removed under reduced pressure, and the product **10a** was purified by PTLC (chloroform/methanol = 9/1) followed by HPLC using condition 1 (t_R: 44 min, 6.3 mg, 4.5% yield). ^{1}H-NMR (CD_3OD) δ: 7.87 (m, 2H), 7.55 (t, *J* = 7.45 Hz, 1H), 7.47 (t, *J* = 7.73 Hz, 2H), 6.77 (s, 2H), 4.42 (m, 1H), 4.10 (m, 2H), 3.49 (t, *J* = 6.87 Hz, 2H), 1.90 (m, 1H), 1.74 (m, 1H), 1.60 (m, 2H), and 1.38 (m, 2H). ESI-MS *m/z*: 388 $[M + H]^+$.

_N_-[2-[[5-(2,5-Dioxo-2,5-dihydro-1_H_-pyrrol-1-yl)pentyl]amino]-2-oxoethyl]-3-iodobenzamide (10b)

To a solution of **9a** (96 mg, 0.24 mmol) in acetonitrile (3 mL) was added **6b** (52 mg, 0.24 mmol) and DIPEA (41 μL). The mixture was stirred at room temperature for 1 h. After extraction with ethyl acetate, the organic layer was dried over sodium sulfate. The solvent was removed under reduced pressure, and the product **10b** was purified by silica gel column chromatography (chloroform/methanol = 10/1, 51 mg, 46% yield). ^{1}H-NMR ($CDCl_3$) δ: 8.18 (t, J = 1.72 Hz, 1H), 7.85 (m, 1H), 7.78 (dd, J = 1.15, 7.45 Hz, 1H), 7.19 (t, J = 7.73 Hz, 1H), 7.05 (s, 1H), 6.69 (s, 2H), 6.13 (s, 1H), 4.10 (d, J = 5.16 Hz, 2H), 3.52 (t, J = 6.87 Hz, 2H), 3.43 (m, 2H), 1.62 (m, 4H), and 1.32 (m,2H). ESI-MS *m/z*: 470 $[M + H]^+$.

(2_S_)-2-[3-[(1_R_)-2-[[1-[(_S_)-5-(2-Benzamidoacetamido)-5-carboxypentyl]-2,5-dioxopyrrolidin-3-yl]thio]-1-carboxyethyl]ureido]pentanedioic acid (11a)

To a solution of **2** (4.8 mg, 0.016 mmol) in H_2O (0.4 mL) was added **10a** (6.3 mg 0.013 mmol) in acetonitrile (0.6 mL). The mixture was neutralized with 2 N NaOH and stirred at room temperature for 1h. **11a** was purified by HPLC using condition 1 (t_R: 37 min, 5.9 mg, 54% yield). ^{1}H-NMR (CD_3OD) δ: 7.88 (m, 2H), 7.55 (t, J = 7.73 Hz, 1H), 7.47 (t, J = 7.45 Hz, 2H), 4.61 (m, 1H), 4.42 (m, 1H), 4.32 (m, 1H), 4.11 (m, 2H), 4.01 (m, 1H), 3.50 (m, 2H), 3.19

(m, 2H), 2.48 (m, 1H), 2.40 (m, 2H), 2.14 (m, 1H), 1.89 (m, 2H), 1.73 (m, 1H), 1.61 (m, 2H), and 1.39 (m, 2H). FAB-MS *m/z*: 682 $[M + H]^+$. HRFAB$^+$-MS: calcd for $C_{28}H_{36}N_5O_{13}S$, 682.2037 $[M + H]^+$; found 682.2030.

(2*S*)-2-[3-[(1*R*)-1-Carboxy-2-[[1-[5-[2-(3-iodobenzamido)acetamido]pentyl]-2,5-dioxopyrrolidin-3-yl]thio]ethyl]ureido]pentanedioic acid (11b)

To a solution of **2** (14 mg, 0.048 mmol) in H_2O (0.3 mL) was added **10b** (23 mg, 0.059 mmol) in acetonitrile (0.3 mL). The mixture was neutralized with 2 N NaOH and stirred at room temperature for 1 h. **11b** was purified by HPLC using condition 2 (t_R: 42 min, 16 mg, 43% yield). ^{1}H-NMR (CD_3OD) δ: 8.26 (t, J = 1.72 Hz, 1H), 7.89 (m, 2H), 7.25 (t, J = 8.02 Hz, 1H), 4.61 (m, 1H), 4.31 (m, 1H), 3.98 (m, 3H), 3.48 (m, 3H), 3.20 (m, 4H), 2.50 (m, 1H), 2.42 (m, 2H), 2.14 (m, 1H), 1.89 (m, 1H), 1.56 (m, 4H), and 1.32 (m, 2H). FAB-MS *m/z*: 764 $[M + H]^+$. HRFAB$^+$-MS: calcd for $C_{27}H_{35}N_5O_{11}SI$, 764.1093 $[M + H]^+$; found 764.1099.

3-(3-Iodobenzamido)propanoic acid (13a)

To a solution of **12** (600 mg, 1.74 mmol) in acetonitrile (6 mL) was added 3-aminopropionic acid (170 mg, 1.91 mmol) and DIPEA (0.33 mL). The mixture was stirred at room temperature for 11 h. After extraction with ethyl acetate and washing with saturated aqueous ammonium

chloride, the organic layer was dried over sodium sulfate. The solvent was removed under reduced pressure, and the resulting precipitate was washed with chloroform to afford **13a** (214 mg, 39% yield). ^{1}H-NMR (CD_3OD) δ: 8.16 (t, *J* = 1.72 Hz, 1H), 7.88 (d, *J* = 6.87 Hz, 1H), 7.79 (m, 1H), 7.23 (t, *J* = 8.02 Hz, 1H), 3.61 (t, *J* = 6.87 Hz, 2H), and 2.62 (t, *J* = 6.87 Hz, 2H). EI-MS *m/z*: 319 $[M]^+$, 231 (36), 203 (12), 76 (36).

4-(3-Iodobenzamido)butanoic acid (13b)

To a solution of **12** (500 mg, 1.45 mmol) in acetonitrile (4 mL) was added 4-aminobutanoic acid (164 mg, 1.59 mmol) and DIPEA (0.27 mL). The mixture was stirred at room temperature overnight. After extraction with ethyl acetate and washing with saturated aqueous ammonium chloride, the organic layer was dried over sodium sulfate. The solvent was removed under reduced pressure, and the resulting precipitate was washed with chloroform to afford **10b** (316 mg, 65% yield). ^{1}H-NMR (CD_3OD) δ: 8.17 (t, *J* = 1.72 Hz, 1H), 7.88 (dt, *J* = 1.72, 8.02 Hz, 1H), 7.80 (dt, J = 1.72, 8.02 Hz, 1H), 7.23 (t, *J* = 8.02 Hz, 1H), 3.41 (t, *J* = 7.16 Hz, 2H), 2.38 (t, *J* = 7.16 Hz, 2H), and 1.90 (tt, *J* = 7.16, 7.16 Hz, 2H). EI-MS *m/z*: 333 $[M]^+$, 274 (19), 231 (36), 102 (50), 76 (51).

5-(3-Iodobenzamido)pentanoic acid (13c)

To a solution of **12** (500 mg, 1.45 mmol) in acetonitrile (6 mL) was added 5-aminopentanoic acid (188 mg, 1.60 mmol) and DIPEA (0.27 mL). The mixture was stirred at room temperature for 7 h. After extraction with ethyl acetate and washing with saturated aqueous ammonium chloride, the organic layer was dried over sodium sulfate. The solvent was removed under reduced pressure, and the resulting precipitate was washed with chloroform to afford **13c** (252 mg, 50% yield). ^{1}H-NMR (CD_3OD) δ: 8.17 (t, J = 1.72 Hz, 1H), 7.87 (dt, J = 1.72, 8.02 Hz, 1H), 7.80 (m, 1H), 7.23 (t, J = 8.02 Hz, 1H), 3.38 (t, J = 6.87 Hz, 2H), 2.35 (t, J = 6.87 Hz, 2H), and 1.66 (m, 4H). EI-MS *m/z*: 347 $[M]^+$, 288 (27), 260 (12), 231 (100), 203 (23), 116 (18), 104 (14), 76 (36).

2,5-Dioxopyrrolidin-1-yl 3-(3-iodobenzamido)propanoate (14a)

To a solution of **13a** (200 mg, 0.63 mmol) in DMF (4 mL) was added NHS (72 mg, 0.63 mmol) and WSCI· HCl (120 mg, 0.63 mmol). The mixture was stirred at room temperature for 7 h. After extraction with ethyl acetate and washing with saturated aqueous sodium bicarbonate, the organic layer was dried over sodium sulfate. The solvent was removed under reduced pressure, and the product **14a** was purified by silica gel column chromatography (chloroform/methanol = 10/1, 93 mg, 36% yield). ^{1}H-NMR ($CDCl_3$, 500 MHz) δ: 8.18 (t, J = 1.72 Hz, 1H), 7.83 (d, J = 8.02 Hz, 1H), 7.76 (d, J = 8.02 Hz, 1H), 7.17 (t, J = 8.02 Hz, 1H),

6.95 (broad s, 1H), 3.88 (m, 2H), 2.94 (t, J = 6.30 Hz, 2H), and 2.88 (s, 4H). EI-MS *m/z*: 416 $[M]^+$, 301 (41), 260 (13), 231 (100), 203 (24), 104 (12), 76 (40).

2,5-Dioxopyrrolidin-1-yl 4-(3-iodobenzamido)butanoate (14b)

To a solution of **13b** (250 mg, 0.75 mmol) in DMF (5 mL) was added NHS (86 mg, 0.75 mmol) and WSCI· HCl (144 mg, 0.75 mmol). The mixture was stirred at room temperature overnight. After extraction with ethyl acetate and washing with saturated aqueous sodium bicarbonate, the organic layer was dried over sodium sulfate. The solvent was removed under reduced pressure, and the product **14b** was purified by silica gel column chromatography (chloroform/methanol = 10/1, 195 mg, 60% yield). ^{1}H-NMR ($CDCl_3$, 500 MHz) δ: 8.10 (t, J = 1.72 Hz, 1H), 7.82 (d, J = 7.45 Hz, 1H), 7.73 (d, J = 7.45 Hz, 1H), 7.17 (t, J = 7.45 Hz, 1H), 6.51 (broad s, 1H), 3.56 (m, 2H), 2.86 (s, 4H), 2.73 (t, J = 6.87 Hz, 2H), and 2.12 (tt, J = 6.87 Hz, 6.87 Hz, 2H). EI-MS *m/z*: 430 $[M]^+$, 315 (36), 274 (8), 231 (100), 203 (25), 104 (13), 84 (26), 76 (42).

2,5-Dioxopyrrolidin-1-yl 5-(3-iodobenzamido)pentanoate (14c)

To a solution of **13c** (133 mg, 0.38 mmol) in DMF (4 mL) was added NHS (44 mg, 0.38 mmol) and WSCI· HCl (73 mg, 0.38 mmol). The mixture was stirred at room temperature for 3

h. After extraction with ethyl acetate and washing with saturated aqueous sodium bicarbonate, the organic layer was dried over sodium sulfate. The solvent was removed under reduced pressure, and the product **14c** was purified by silica gel column chromatography (chloroform/methanol = 20/1, 83 mg, 49% yield). ^{1}H-NMR ($CDCl_3$, 500 MHz) δ: 8.10 (t, J = 1.72 Hz, 1H), 7.81 (d, J = 8.02 Hz, 1H), 7.75 (d, J = 8.02 Hz, 1H), 7.17 (t, J = 8.02 Hz, 1H), 6.36 (broad s, 1H), 3.50 (m ,2H), 2.86 (s, 4H), 2.69 (t, J = 6.87 Hz, 2H), 1.88 (m, 2H), and 1.76 (m, 2H). EI-MS *m/z*: 444 $[M]^+$, 330 (7), 288 (18), 231 (100), 203 (20), 104 (14), 98 (16), 76 (32).

(*S*)-6-(2,5-Dioxo-2,5-dihydro-1*H*-pyrrol-1-yl)-2-(3-(3-iodobenzamido)propanamido)hexanoic acid (15a)

To a solution of **14a** (110 mg, 0.26 mmol) in acetonitrile (3 mL) was added **6a** (69 mg, 0.26 mmol) and DIPEA (91 μL). The mixture was stirred at room temperature for 4 h. After extraction with ethyl acetate and washing with saturated aqueous ammonium chloride, the organic layer was dried over sodium sulfate. The solvent was removed under reduced pressure, and the product **15a** was purified by PTLC (chloroform/methanol = 10/1) followed by HPLC using condition 1 (t_R: 60 min, 19 mg, 14% yield). ^{1}H-NMR（CD_3OD, 500 MHz）δ: 8.17 (t, J = 1.72 Hz, 1H), 7.87 (d, J = 8.02 Hz, 1H), 7.81 (d, J = 8.02 Hz, 1H), 7.22 (t, J = 8.02 Hz, 1H),

6.78 (s, 2H), 4.36 (m, 1H), 3.64 (m, 2H), 3.44 (t, J = 7.16 Hz, 2H), 2.56 (m, 2H), 1.66–1.89 (m, 2H), 1.57 (m, 2H), and 1.35 (m, 2H). ESI-MS *m/z*: 528 $[M + H]^+$.

(*S*)-6-(2,5-Dioxo-2,5-dihydro-1*H*-pyrrol-1-yl)-2-(4-(3-iodobenzamido)butanamido)hexanoic acid (15b)

To a solution of **14b** (58 mg, 0.13 mmol) in acetonitrile (2 mL) was added **6a** (35 mg, 0.13 mmol) and DIPEA (46 μL). The mixture was stirred at room temperature for 4 h. After extraction with ethyl acetate and washing with saturated aqueous ammonium chloride, the organic layer was dried over sodium sulfate. The solvent was removed under reduced pressure, and the product **15b** was purified by PTLC (chloroform/methanol = 10/1) followed by HPLC using condition 1 (t_R: 62 min, 12 mg, 17% yield). ^{1}H-NMR（CD_3OD, 500 MHz）δ: 8.18 (t, J = 1.72 Hz, 1H), 7.88 (d, J = 8.02 Hz, 1H), 7.82 (d, J = 8.02 Hz, 1H), 7.24 (t, J = 8.02 Hz, 1H), 6.78 (s, 2H), 4.34 (m, 1H), 3.49 (t, J = 6.87 Hz, 2H), 3.41 (t, J = 6.87 Hz, 2H), 2.33 (t, J = 7.45 Hz, 2H), 1.92 (t, J = 6.87 Hz, 2H), 1.67–1.91 (m, 2H), 1.59 (m, 2H), and 1.36 (m, 2H). ESI-MS *m/z*: 542 $[M + H]^+$.

(*S*)-6-(2,5-Dioxo-2,5-dihydro-1*H*-pyrrol-1-yl)-2-(5-(3-iodobenzamido)pentanamido)hexanoic acid (15c)

To a solution of **14c** (100 mg, 0.23 mmol) in acetonitrile (2 mL) was added **6a** (60 mg, 0.23 mmol) and DIPEA (77 μL). The mixture was stirred at room temperature for 2 h. After extraction with ethyl acetate and washing with saturated aqueous ammonium chloride, the organic layer was dried over sodium sulfate. The solvent was removed under reduced pressure, and the product **15c** was purified by PTLC (chloroform/methanol = 10/1) followed by HPLC using condition 1 (t_R: 63 min, 30 mg, 24% yield). ^{1}H-NMR（CD_3OD, 500 MHz）δ: 8.17 (t, J = 1.72 Hz, 1H), 7.87 (d, J = 8.02 Hz, 1H), 7.81 (d, J = 8.02 Hz, 1H), 7.23 (t, J = 8.02 Hz, 1H), 6.78 (s, 2H), 4.35 (m, 1H), 3.48 (t, J = 7.16 Hz, 2H), 3.39 (m, 2H), 2.30 (t, J = 7.16 Hz, 2H), 1.55–1.86 (m, 8H), and 1.36 (m, 2H). ESI-MS *m/z*: 556 $[M + H]^+$.

(2*S*)-2-(3-(1*R*)-1-Carboxy-2-((1-(*S*)-5-carboxy-5-(3-(3-iodobenzamido)propanamido)pentyl-2,5-dioxopyrrolidin-3-yl)thio)ethyl)ureido)pentanedioic acid (16a)

To a solution of **2** (6.1 mg, 0.021 mmol) in H_2O (0.6 mL) was added **15a** (11 mg, 0.021 mmol) in acetonitrile (0.4 mL). The mixture was neutralized with 2 N NaOH and stirred at room temperature for 2 h. The product **16a** was purified by HPLC using condition 1 (t_R: 52 min, 10 mg, 58% yield). ^{1}H-NMR (CD_3OD, 500 MHz) δ: 8.18 (t, J = 1.72 Hz, 1H), 7.87 (t, J = 8.02 Hz, 1H), 7.81 (d, J = 8.02 Hz, 1H), 7.23 (t, J = 8.02 Hz, 1H), 4.53 (m, 1H), 4.37 (m, 1H), 4.01 (m, 1H), 3.65 (m, 2H), 3.39 (m, 2H), 3.22 (m, 2H), 2.58 (m, 2H), 2.41 (m, 2H), 2.15 (m,

2H), 1.88 (m, 2H), 1.70 (m, 1H), 1.56 (m, 2H), and 1.35 (m, 2H). FAB-MS *m/z*: 822 $[M + H]^+$. HRFAB$^+$-MS: calcd for $C_{29}H_{37}N_5O_{13}SI$, 822.1159 $[M + H]^+$; found 822.1153.

(2*S*)-2-(3-(1*R*)-1-Carboxy-2-((1-(*S*)-5-carboxy-5-(4-(3-iodobenzamido)butanamido)pentyl-2,5-dioxopyrrolidin-3-yl)thio)ethyl)ureido)pentanedioic acid (16b)

To a solution of **2** (6.0 mg, 0.020 mmol) in H_2O (0.9 mL) was added **15b** (11 mg, 0.020 mmol) in acetonitrile (0.9 mL). The mixture was neutralized with 2 N NaOH and stirred at room temperature for 1 h. The product **16b** was purified by HPLC using condition 1 (t_R: 53 min, 12 mg, 73% yield). ^{1}H-NMR (CD_3OD, 500 MHz) δ: 8.19 (t, *J* = 1.72 Hz, 1H), 7.88 (t, *J* = 8.02 Hz, 1H), 7.82 (d, *J* = 8.02 Hz, 1H), 7.24 (t, *J* = 8.02 Hz, 1H), 4.61 (m, 1H), 4.33 (m, 2H), 4.00 (m, 1H), 3.49 (m, 2H), 3.42 (t, *J* = 6.87 Hz, 2H), 3.35 (s, 1H), 3.19 (m, 2H), 2.40 (m, 2H), 2.34 (t, *J* = 7.45 Hz, 2H), 2.15 (m, 1H), 1.90 (m, 4H), 1.69 (m, 2H), and 1.49 (m, 2H). FAB-MS *m/z*: 836 $[M + H]^+$. HRFAB$^+$-MS: calcd for $C_{30}H_{39}N_5O_{13}SI$, 836.1310 $[M + H]^+$; found 836.1315.

(2*S*)-2-(3-(1*R*)-1-Carboxy-2-((1-(*S*)-5-carboxy-5-(5-(3-iodobenzamido)pentanamido)pentyl-2,5-dioxopyrrolidin-3-yl)thio)ethyl)ureido)pentanedioic acid (16c)

To a solution of **2** (9.0 mg, 0.031 mmol) in H_2O (0.6 mL) was added **15c** (17 mg, 0.031

mmol) in acetonitrile (1 mL). The mixture was neutralized with 2 N NaOH and stirred at room temperature for 2 h. The product **16c** was purified by HPLC using condition 1 (t_R: 55 min, 6 mg, 23% yield). ^{1}H-NMR (CD_3OD, 500 MHz) δ: 8.17 (t, J = 1.72 Hz, 1H), 7.87 (t, J = 8.02 Hz, 1H), 7.81 (d, J = 8.02 Hz, 1H), 7.23 (t, J = 8.02 Hz, 1H), 4.62 (m, 1H), 4.33 (m, 2H), 4.00 (m, 1H), 3.47 (m, 2H), 3.39 (m, 2H), 3.19 (m, 2H), 2.47 (m, 1H), 2.40 (m, 2H), 2.31 (t, J = 6.87 Hz, 2H), 2.16 (m, 1H), 1.88 (m, 2H), 1.64–1.73 (m, 5H), 1.60 (m, 2H), and 1.38 (m, 2H). FAB-MS *m/z*: 850 $[M + H]^+$. HRFAB$^+$-MS: calcd for $C_{31}H_{41}N_5O_{13}SI$, 850.1461 $[M + H]^+$; found 850.1466.

(*S*)-6-(2,5-Dioxo-2,5-dihydro-1*H*-pyrrol-1-yl)-2-(3-iodobenzamido)hexanoic acid (17)

To a solution of **12** (80 mg, 0.23 mmol) in acetonitrile (1.8 mL) was added **6a** (61 mg, 0.23 mmol) and DIPEA (80 μL). The mixture was stirred at room temperature for 5 h. After extraction with ethyl acetate and washing with saturated aqueous ammonium chloride, the organic layer was dried over sodium sulfate. The solvent was removed under reduced pressure, and the product **17** was purified by PTLC (chloroform/methanol = 9/1, 25 mg, 26% yield). ^{1}H-NMR ($CDCl_3$, 500 MHz) δ: 8.17 (s, 1H), 7.82 (t, J = 8.02 Hz, 1H), 7.79 (d, J = 8.02 Hz, 1H), 7.16 (t, J = 7.73 Hz, 1H), 6.96 (broad s, 1H), 6.69 (s, 2H), 4.64 (s, 1H), 3.53 (t, J = 6.87 Hz, 2H), 1.87–2.03 (m, 2H), 1.64 (m, 2H), and 1.33–1.42 (m, 2H). ESI-MS *m/z*: 457 $[M + H]^+$.

(2*S*)-2-(3-((1*R*)-1-Carboxy-2-((1-((*S*)-5-carboxy-5-(3-iodobenzamido)pentyl-2,5-dioxopyrrolidin-3-yl)thio)ethyl)ureido)pentanedioic acid (18)

To a solution of **2** (10 mg, 0.034 mmol) in H_2O (0.7 mL) was added **17** (15.5 mg, 0.034 mmol) in acetonitrile (0.2 mL). The mixture was neutralized with 2 N NaOH and stirred at room temperature for 2 h. **18** was purified by HPLC using condition 1 (t_R: 53 min, 11 mg, 43% yield). ^{1}H-NMR (D_2O, 500 MHz) δ: 8.06 (s, 1H), 7.90 (d, J = 8.02 Hz, 1H), 7.69 (d, J = 8.02 Hz, 1H), 7.21 (t, J = 8.02 Hz, 1H), 4.46 (m, 1H), 4.37 (m, 1H), 4.18 (m, 1H), 3.88 (m, 1H), 3.45 (t, J = 6.30 Hz, 2H), 2.76–3.18 (m, 3H), 2.40 (m, 2H), 2.07 (m, 1H), 1.73–1.96 (m, 3H), 1.56 (m, 2H), and 1.29 (m, 2H). FAB-MS *m/z*: 751 $[M + H]^+$. HRFAB$^+$-MS: calcd for $C_{26}H_{32}N_4O_{12}SI$, 751.0786 $[M + H]^+$; found 751.0782.

(*2S*)-2-[3-[(*1R*)-1-Carboxy-2-[(1-methyl-2,5-dioxopyrrolidine-3-yl)thio]ethyl]ureido]pentanedioic acid (19)

To a solution of **2** (10.6 mg, 0.036 mmol) in H_2O (0.5 mL) was added *N*-methylmaleimide (4.0 mg, 0.036 mmol) in acetonitrile (0.2 mL). The mixture was neutralized with 2 N NaOH and stirred at room temperature for 2 h. Product **19** was purified by HPLC using condition 1 (t_R: 21 min, 6.5 mg, 45% yield). ^{1}H-NMR (D_2O, 500 MHz) δ: 4.44 (m, 1H), 4.17 (m, 1H), 3.96

(m 1H), 3.18 (m, 1H), 3.12 (m, 2H), 2.85 (s, 3H), 2.59 (m, 1H), 2.41 (t, *J* = 7.45 Hz, 2H), 2.08 (m, 1H), and 1.87 (m, 1H). FAB-MS *m/z*: 406 $[M + H]^+$. HRFAB$^+$-MS: calcd for $C_{14}H_{20}N_3O_9S$, 406.0924 $[M + H]^+$; found 406.0920.

(*S*)-2-((1-Carboxy-5-(2,5-dioxo-2,5-dihydro-1*H*-pyrrol-1-yl)pentyl)amino-*N*-methyl-2-oxo ethanaminium chloride (21)

To a solution of **20** (290 mg, 1.01 mmol) in acetonitrile (4 mL) was added **6a** (277 mg, 1.05 mmol) and DIPEA (0.23 mL). The mixture was stirred at room temperature for 2 h. After extraction with ethyl acetate and washing with saturated aqueous ammonium chloride, the organic layer was dried over sodium sulfate. The solvent was removed under reduced pressure, and the product was partially purified by PTLC (chloroform/methanol = 9/1). ESI-MS *m/z*: 420 $[M + Na]^+$. Next, the *tert*-butoxycarbonyl group was removed by treatment with 4 N HCl/ethyl acetate. The precipitate was washed with ethyl acetate and purified by HPLC using condition 1 to yield **21** (t_R: 22 min, 15 mg, 4% yield; 2 steps). ^{1}H-NMR (D_2O, 500 MHz) δ: 6.80 (s, 2H), 4.43 (m, 1H), 3.83 (broad s, 2H), 3.50 (t, *J* = 6.87 Hz, 2H), 2.73 (s, 3H), 1.92 (m, 1H), 1.73 (m, 1H), 1.61 (m, 2H), and 1.38 (m, 2H). ESI-MS *m/z*: 298 $[M + H]^+$.

(2*S*)-2-(3-((1*R*)-1-Carboxy-2-((1-((*S*)-5-carboxy-5-(2-(methylamino)acetamido)pentyl-2,5-

dioxopyrrolidin-3-yl)thio)ethyl)ureido)pentanedioic acid (22)

To a solution of **2** (6.8 mg, 0.023 mmol) in H_2O (0.3 mL) was added **21** (6.9 mg, 0.021 mmol). The mixture was neutralized with 2 N NaOH and stirred at room temperature for 2 h. The product **22** was purified by HPLC using condition 1 (t_R: 20 min, 7 mg, 52% yield). ^{1}H-NMR (D_2O, 500 MHz) δ: 4.43 (m, 1H), 4.28 (dd, J = 5.16 Hz, 8.59 Hz, 2H), 4.17 (m, 1H), 3.95 (m, 1H), 3.82 (s, 2H), 3.40 (t, J = 6.87 Hz, 2H), 2.95–3.26 (m, 4H), 2.66 (s, 3H), 2.59 (m, 1H), 2.40 (t, J = 7.14 Hz, 2H), 2.08 (m, 1H), 1.83 (m, 2H), 1.65 (m, 1H), 1.48 (m, 2H), and 1.23 (m, 2H). FAB-MS *m/z*: 592 $[M + H]^+$. HRFAB$^+$-MS: calcd for $C_{22}H_{34}N_5O_{12}S$, 592.1929 $[M + H]^+$; found 592.1925.

Cell Lines and Mouse Models

Two human prostate carcinoma cell lines were purchased from DS PHARMA BIOMEDICAL (Osaka, Japan): LNCaP (PSMA positive) and PC-3 (PSMA negative).[12] The cells were cultured as previously reported in Roswell Park Memorial Institute 1640 (RPMI 1640) medium supplemented with 10% fetal bovine serum, glutamine, and antibiotics (penicillin/streptomycin) in a humidified CO_2 incubator (37 °C/5% CO_2).[15]

C.B.-17/Icr +/+ Jcl mice and C.B.-17/Icr *scid/scid* Jcl mice were purchased from CLEA Japan (Tokyo, Japan). Animal studies were conducted in accordance with the guidelines of our

institution: “Regulation on Animal Experimentation at Kyoto University”. Cultured cells were treated with 2.5 g/L trypsin/1 mM ethylenediaminetetraacetic acid and were re-suspended in phosphate buffered saline. Each mouse was injected with 100 μL of a 1:1 mixture of cell suspension and BD Matrigel™ Basement Membrane Matrix (1–5 × 10^6 cells/mouse) in the right (PC-3) or left (LNCaP) shoulder. Tumor-bearing mice were used for studies when tumors reached a diameter of approximately 5–10 mm.

***In Vitro* Cell-binding Assay (Saturation Assay)**

The affinity of [^{125}I]**3** for PSMA was determined by an *in vitro* saturation assay according to previous reports with slight modifications.[28, 32] LNCaP cells in 12-well plates (4 × 10^5 cells/well) were incubated for 48 h (37 °C/5% CO_2). The medium was removed, and each well was washed twice with 500 μL of assay medium (RPMI 1640 supplemented with 0.5% bovine serum albumin). The ^{125}I-labeled compound (specific activity; 81.4 kBq/nmol) was added to each well, and the plates were incubated at 37 °C for 1 h. Non-specific binding was evaluated by adding 100 μM of non-radioactive iodinated test compound. After incubation, each well was washed twice with 500 μL of fresh assay medium, and the cells were lysed with 0.2 N NaOH. Radioactivity bound to cells was measured with a γ-counter. K_d values were calculated using Scatchard plots.

In Vitro Cell-Binding Assay (Inhibition Assay)

The affinities of the novel compounds **11a**–**11b**, **16a**–**16c**, **18**, **19**, **22**, and **3** were determined by an *in vitro* binding inhibition assay, as previously reported with slight modification.[32] [^{125}I]**23** was used as the radioligand for the inhibition assay. LNCaP cells in 12-well plates (4×10^5 cells/well) were incubated for 48 h (37 °C/5% CO_2). The medium was removed, and then each well was washed twice with 500 μL of assay medium (RPMI 1640 supplemented with 0.5% bovine serum albumin). 500 μL of [^{125}I]**23** (29.6 kBq/mL) and the test compound were added to each well, and the plates were incubated at 37 °C for 1 h. Non-specific binding was evaluated by adding 0.5 mM 2-PMPA (Tocris Bioscience, Missouri, USA). After incubation, each well was washed twice with 500 μL of fresh assay medium, and then the cells were lysed with 0.2 N NaOH. Radioactivity bound to the cells was measured with a γ-counter. IC_{50} values were calculated using the GraphPad Prism 5 program (GraphPad Software, Inc., San Diego, CA, USA). K_i values were calculated using the Cheng-Prusoff equation.[35]

In Vitro Stability

C.B.-17/Icr +/+ Jcl male mice weighing 20–22 g were anesthetized with isoflurane. Blood samples were collected from the hearts and were centrifuged at 1,500 × *g*. The supernatant was

collected and stored at −80 °C until use. Twenty μL of [^{125}I]**3** was added to 100 μL of mouse serum. The sample was incubated at 37 °C for 1, 3, or 6 h. After incubation, 150 μL of methanol was added to the sample, and it was centrifuged at 5,000 × *g*. The supernatant was collected and filtered with a Cosmonice Filter (S) (0.45 μm, 4 mm), and the filtrate was analyzed by HPLC.

Biodistribution and Blocking Studies

100 μL of [^{125}I]**3** was administered by injection to tumor bearing mice weighing 22–24 g via the tail vein (n=4 for each time point). Mice were sacrificed by decapitation at the following fixed time points: 2 min, 30 min, 1 h, 3 h, and 6 h. The weight and radioactivity of tissues were measured, and the uptake of [^{125}I]**3** was evaluated as a percentage of the injected dose per gram of tissue (%ID/g).

To confirm *in vivo* PSMA-specific binding, a blocking study was conducted. Briefly, 100 μL of [^{125}I]**3** was coinjected with 2-PMPA (50 mg/kg weight), a GCP-II inhibitor, to tumor-bearing mice weighing 22–24 g via the tail vein. The mice were decapitated 30 min after injection. The weight and radioactivity of each tissue were measured, and the uptake of [^{125}I]**3** was evaluated as %ID/g.

Small-animal SPECT/CT

SPECT/CT studies were performed using the FX3300 imager (SII NanoTechnology Inc., Northridge, CA, USA). LNCaP and PC-3 tumor-bearing mice (20–25 g) were anesthetized (2.5% isoflurane in an air mixture) and placed on a heating pad to maintain body temperature. The mice were then injected with [^{123}I]**3** (25.9 MBq, in 0.10 mL isotonic saline) via the tail vein. A competition experiment was performed by coinjection of the radiotracer with 50 mg/kg of 2-PMPA in a total volume of 0.10 mL of isotonic saline.

SPECT scans were acquired over 30–64 min, after which CT scans were performed for anatomic reference (spatial resolution, 50 μm; 60 kV; and 310 μA). In the SPECT studies, all projection data were acquired using a 20% energy window centered at 159 keV for ^{123}I, a 35 mm radius of rotation, a 360° circular orbit, a 60 s projection time, and 32 projection angles. Single-pinhole collimators (1.0 mm diameter, 9.0 mm focal length) were used. SPECT images were reconstructed using three-dimensional ordered-subset expectation maximization, and CT images were reconstructed using a modified three-dimensional cone-beam Feldkamp algorithm resulting in a 0.177 × 0.177 × 0.177 mm voxel size for a 512 × 512 × 512 image volume. Acquired SPECT and CT datasets were processed with AMIRA software (version 5.1) (FEI Company, Hillsboro, Oregon, USA).

Statistics

GraphPad Prism 5 software was used for statistical analyses. The Tukey–Kramer test was used to assess statistical differences. A P value < 0.05 was considered statistically significant.

ASSOCIATED CONTENT

Supporting Information

Docking simulation study, additional data of radiosynthesis and biodistribution, reverse phase HPLC retention time, and distribution coefficient. This material is available free of charge via the Internet at http://pubs.acs.org.

AUTHOR INFORMATION

*Phone: +81-75-753-4566. Fax: +81-75-753-4568. E-mail: hsaji@pharm.kyoto-u.ac.jp

ACKNOWLEDGMENTS

This work was partly supported by a Grant-in-Aid for Young Scientists (B) from the Japan Society for the Promotion of Science, and New Energy and Industrial Technology Development Organization (NEDO). No potential conflict of interest relevant to this article is reported.

ABBREVIATION USED

PSMA, prostate-specific membrane antigen; 2-PMPA, 2-(phosphonomethyl)pentanedioic acid; PSA, prostate specific antigen; BPH, benign prostatic hyperplasia; PET, positron emission tomography; SPECT, single photon emission computed tomography; [^{18}F]FDG,

2-deoxy-2-[^{18}F]fluoro-D-glucose; GCP-II, glutamate carboxypeptidase-II; NMR, nuclear magnetic resonance; FAB, fast atom bombardment; HRMS, high-resolution mass spectrometry; HPLC, high-performance liquid chromatography; log D, distribution coefficient; PTLC, preparative thin layer chromatography; TFA, trifluoroacetic acid; DMSO, dimethylsulfoxide; ESI, electrospray ionization; MS, mass spectrometry; DMF, *N,N*-dimethylformamide; H-Gly-OPMB, 4-methoxybenzyl 2-aminoacetate hydrochloride; WSCI· HCl, water soluble carbodiimide hydrochloride; NHS, *N*-hydroxysuccinimide; DIC, *N,N´*-diisopropylcarbodiimide; DIPEA, *N,N*-diisopropylethylamine

REFERENCES

1. Siegel, R.; Naishadham, D.; Jemal, A. Cancer Statistics, 2012. *Ca–Cancer J. Clin.* **2012**, *62*, 10–29.

2. Cook, E.; Nelson, A. Prostate Cancer Screening. *Curr. Oncol. Rep.* **2011**, *13*, 57–62.

3. Hugosson, J.; Carlsson, S.; Aus, G.; Bergdahl, S.; Khatami, A.; Lodding, P.; Pihl, C.; Stranne, J.; Holmberg, E.; Lilja, H. Mortality results from the Goteborg randomised population-based prostate-cancer screening trial. *Lancet Oncol.* **2010**, *11*, 725–732.

4. Stamey, T.; Yang, N.; Hay, A.; Mcneal, J.; Freiha, F.; Redwine, E. Prostate-Specific Antigen As a Serum Marker For Adenocarcinoma Of The Prostate. *New Engl. J. Med.* **1987**, *317*, 909–916.

5. Effert, P.; Bares, R.; Handt, S.; Wolff, J.; Bull, U.; Jakse, G. Metabolic imaging of untreated prostate cancer by positron emission tomography with (18)fluorine-labeled deoxyglucose. *J. Urology* **1996**, *155*, 994–998.

6. Hain, S.; Maisey, M. Positron emission tomography for urological tumours. *Bju Int.* **2003**, *92*, 159–164.

7. Bouchelouche, K.; Tagawa, S.; Goldsmith, S.; Turkbey, B.; Capala, J.; Choyke, P. PET/CT Imaging and Radioimmunotherapy of Prostate Cancer. *Semin. Nucl. Med.* **2011**, *41*, 29–44.

8. Liu, I.; Zafar, M.; Lai, Y.; Segall, G.; Terris, M. Fluorodeoxyglucose positron emission tomography studies in diagnosis and staging of clinically organ-confined prostate cancer. *Urol.* **2001**, *57*, 108–111.

9. Barinka, C.; Rojas, C.; Slusher, B.; Pomper, M. Glutamate Carboxypeptidase II in Diagnosis and Treatment of Neurologic Disorders and Prostate Cancer. *Curr. Med. Chem.* **2012**, *19*, 856–870.

10. Silver, D.; Pellicer, I.; Fair, W.; Heston, W.; CordonCardo, C. Prostate-specific membrane antigen expression in normal and malignant human tissues. *Clin. Cancer Res.* **1997**, *3*, 81–85.

11. Su, S.; Huang, I.; Fair, W.; Powell, C.; Heston, W. Alternatively Spliced Variants of Prostate-Specific Membrane Antigen RNA - Ratio of Expression As a Potential Measurement of Progression. *Cancer Res.* **1995**, *55*, 1441–1443.

12. Israeli, R.; Powell, C.; Fair, W.; Heston, W. Molecular-Cloning of a Complementary-DNA Encoding a Prostate-Specific Membrane Antigen. *Cancer Res.* **1993**, *53*, 227–230.

13. Ponsky, L.; Cherullo, E.; Starkey, R.; Nelson, D.; Neumann, D.; Zippe, C. Evaluation of preoperative ProstaScint (TM) scans in the prediction of nodal disease. *Prostate Cancer Prostatic Dis.* **2002**, *5*, 132–135.

14. Liu, H.; Moy, P.; Kim, S.; Xia, Y.; Rajasekaran, A.; Navarro, V.; Knudsen, B.; Bander, N. Monoclonal antibodies to the extracellular domain of prostate-specific membrane antigen also react with tumor vascular endothelium. *Cancer Res.* **1997**, *57*, 3629–3634.

15. Carter, R.; Feldman, A.; Coyle, J. Prostate-specific membrane antigen is a hydrolase with substrate and pharmacologic characteristics of a neuropeptidase. *Proc. Natl. Acad. Sci. U.S.A.* **1996**, *93*, 749–753.

16. Tiffany, C.; Lapidus, R.; Merion, A.; Calvin, D.; Slusher, B. Characterization of the enzymatic activity of PSM: Comparison with brain NAALADase. *Prostate* **1999**, *39*, 28–35.

17. Banerjee, S.; Foss, C.; Castanares, M.; Mease, R.; Byun, Y.; Fox, J.; Hilton, J.; Lupold, S.; Kozikowski, A.; Pomper, M. Synthesis and evaluation of technetium-99m-and rhenium-labeled inhibitors of the prostate-specific membrane antigen (PSMA). *J. Med. Chem.* **2008**, *51*, 4504–4517.

18. Barinka, C.; Rovenska, M.; Mlcochova, P.; Hlouchova, K.; Plechanovova, A.; Majer, P.; Tsukamoto, T.; Slusher, B.; Konvalinka, J.; Lubkowski, J. Structural insight into the pharmacophore pocket of human glutamate carboxypeptidase II. *J. Med. Chem.* **2007,** *50*, 3267–3273.

19. Barinka, C.; Byun, Y.; Dusich, C.; Banerjee, S.; Chen, Y.; Castanares, M.; Kozikowski, A.; Mease, R.; Pomper, M.; Lubkowski, J. Interactions between Human

Glutamate Carboxypeptidase II and Urea-Based Inhibitors: Structural Characterization. *J. Med. Chem.* **2008**, *51*, 7737–7743.

20. Kozikowski, A.; Zhang, J.; Nan, F.; Petukhov, P.; Grajkowska, E.; Wroblewski, J.; Yamamoto, T.; Bzdega, T.; Wroblewska, B.; Neale, J. Synthesis of urea-based inhibitors as active site probes of glutamate carboxypeptidase II: Efficacy as analgesic agents. *J. Med. Chem.* **2004**, *47*, 1729–1738.

21. Banerjee, S.; Pullambhatla, M.; Byun, Y.; Green, G.; Fox, J.; Horti, A.; Mease, R.; Pomper, M. Ga-68-and In-111-Labelled Small Molecule Inhibitors of PSMA for Prostate Cancer Imaging. *J. Label. Compd. Radiopharm.* **2009**, *52*, S19.

22. Banerjee, S.; Pullambhatla, M.; Byun, Y.; Nimmagadda, S.; Green, G.; Fox, J.; Horti, A.; Mease, R.; Pomper, M. Ga-68-Labeled Inhibitors of Prostate-Specific Membrane Antigen (PSMA) for Imaging Prostate Cancer. *J. Med. Chem.* **2010**, *53*, 5333–5341.

23. Eder, M.; Schafer, M.; Bauder-Wust, U.; Hull, W.; Wangler, C.; Mier, W.; Haberkorn, U.; Eisenhut, M. Ga-68-Complex Lipophilicity and the Targeting Property of a Urea-Based PSMA Inhibitor for PET Imaging. *Bioconjugate Chem.* **2012**, *23*, 688–697.

24. Lu, G.; Maresca, K.; Hillier, S.; Zimmerman, C.; Eckelman, W.; Joyal, J.; Babich, J. Synthesis and SAR of Tc-99m/Re-labeled small molecule prostate specific membrane antigen inhibitors with novel polar chelates. *Bioorg. Med. Chem. Lett.* **2013**, *23*, 1557–1563.

25. Nedrow-Byers, J.; Moore, A.; Ganguly, T.; Hopkins, M.; Fulton, M.; Benny, P.; Berkman, C. PSMA-targeted SPECT agents: Mode of binding effect on in vitro performance. *Prostate* **2013**, *73*, 355–362.

26. Kularatne, S.; Zhou, Z.; Yang, J.; Post, C.; Low, P. Design, Synthesis, and Preclinical Evaluation of Prostate-Specific Membrane Antigen Targeted Tc-99m-Radioimaging Agents. *Mol. Pharm.* **2009**, *6*, 790–800.

27. Foss, C.; Mease, R.; Fan, H.; Wang, Y.; Ravert, H.; Dannals, R.; Olszewski, R.; Heston, W.; Kozikowski, A.; Pomper, M. Radiolabeled small-molecule ligands for prostate-specific membrane antigen: In vivo imaging in experimental models of prostate cancer. *Clin. Cancer Res.* **2005**, *11*, 4022–4028.

28. Hillier, S.; Maresca, K.; Femia, F.; Marquis, J.; Foss, C.; Nguyen, N.; Zimmerman, C.; Barrett, J.; Eckelman, W.; Pomper, M.; Joyal, J.; Babich, J. Preclinical Evaluation of Novel Glutamate-Urea-Lysine Analogues That Target Prostate-Specific Membrane Antigen as Molecular Imaging Pharmaceuticals for Prostate Cancer. *Cancer Res.* **2009**, *69*, 6932–6940.

29. Barrett, J.; Coleman, R.; Goldsmith, S.; Vallabhajosula, S.; Petry, N.; Cho, S.; Armor, T.; Stubbs, J.; Maresca, K.; Stabin, M.; Joyal, J.; Eckelman, W.; Babich, J. First-in-Man Evaluation of 2 High-Affinity PSMA-Avid Small Molecules for Imaging Prostate Cancer. *J. Nucl. Med.* **2013**, *54*, 380–387.

30. Wakisaka, K.; Arano, Y.; Uezono, T.; Akizawa, H.; Ono, M.; Kawai, K.; Ohomomo, Y.; Nakayama, M.; Saji, H. A novel radioiodination reagent for protein radiopharmaceuticals with L-lysine as a plasma-stable metabolizable linkage to liberate m-iodohippuric acid after lysosomal proteolysis. *J. Med.Chem.* **1997**, *40*, 2643–2652.

31. Mease, R.; Dusich, C.; Foss, C.; Ravert, H.; Dannals, R.; Seidel, J.; Prideaux, A.; Fox, J.; Sgouros, G.; Kozikowski, A.; Pomper, M. N-[N-[(S)-1,3-dicarboxypropyl]carbamoyl]-4-[F-18]fluorobenzyl-L-cysteine, [F-18]DCFBC: A new imaging probe for prostate cancer. *Clin. Cancer Res.* **2008**, *14*, 3036–3043.

32. Maresca, K.; Hillier, S.; Femia, F.; Keith, D.; Barone, C.; Joyal, J.; Zimmerman, C.; Kozikowski, A.; Barrett, J.; Eckelman, W.; Babich, J. A Series of Halogenated Heterodimeric Inhibitors of Prostate Specific Membrane Antigen (PSMA) as Radiolabeled Probes for Targeting Prostate Cancer. *J. Med. Chem.* **2009**, *52*, 347–357.

33. Majumdar, S.; Burgman, M.; Haselton, N.; Grinnell, S.; Ocampo, J.; Pasternak, A.; Pasternak, G. Generation of novel radiolabeled opiates through site-selective iodination. *Bioorg. Med. Chem. Lett.* **2011**, *21*, 4001–4004.

34. Camphausen, K.; Sproull, M.; Tantama, S.; Venditto, V.; Sankineni, S.; Scott, T.; Brechbiel, M. Evaluation of chelating agents as anti-angiogenic therapy through copper chelation. *Bioorg. Med. Chem.* **2004**, *12*, 5133–5140.

35. Cheng, Y.; Prusoff, W. Relationship Between Inhibition Constant (K1) and Concentration of Inhibitor Which Causes 50 Per Cent Inhibition (I50) of an Enzymatic-Reaction. *Biochem. Pharmacol.* **1973**, *22*, 3099–3108.

36. Mesters, J.; Barinka, C.; Li, W.; Tsukamoto, T.; Majer, P.; Slusher, B.; Konvalinka, J.; Hilgenfeld, R. Structure of glutamate carboxypeptidase II, a drug target in neuronal damage and prostate cancer. *Embo J.* **2006**, *25*, 1375–1384.

37. Barinka, C.; Starkova, J.; Konvalinka, J.; Lubkowski, J. A high-resolution structure of ligand-free human glutamate carboxypeptidase II. *Acta Crystallogr. F-Struct. Biol. Cryst. Commun.* **2007**, *63*, 150–153.

38. Afshar-Oromieh, A.; Haberkorn, U.; Eder, M.; Eisenhut, M.; Zechmann, C. [Ga-68]Gallium-labelled PSMA ligand as superior PET tracer for the diagnosis of prostate cancer: comparison with F-18-FECH. *Eur. J. Nucl. Med. Mol. Imaging* **2012**, *39*, 1085–1086.

39. Afshar-Oromieh, A.; Malcher, A.; Eder, M.; Eisenhut, M.; Linhart, H.; Hadaschik, B.; Holland-Letz, T.; Giesel, F.; Kratochwil, C.; Haufe, S.; Haberkorn, U.; Zechmann, C. PET imaging with a [Ga-68]gallium-labelled PSMA ligand for the diagnosis of prostate cancer: biodistribution in humans and first evaluation of tumour lesions. *Eur. J. Nucl. Med. Mol. Imaging* **2013**, *40*, 486–495.

Table 1. Comparison of affinities between [^{125}I]**3** and previously reported probes

	K_d [nM]
[^{125}I]**3**	7.8 ± 1.4*†
[^{125}I]**23**	143 ± 2
[^{125}I]**24**	20.4 ± 0.6*

Data are expressed as means ± standard deviation. The affinity of [^{125}I]**3** was significantly higher than that of [^{125}I]**3** (*$P < 0.05$) and [^{125}I]**24** ($^{\dagger}P < 0.05$).

Table 2. Comparison of affinities among **3** and its derivatives.

	K_i [nM]
2-PMPA	31.2 ± 7.09
2	376 ± 195
3	4.97 ± 2.66
8a	8.06 ± 3.07
8b	7.91 ± 2.67
13a	6.26 ± 4.87
13b	2.95 ± 0.29
13c	2.14 ± 0.77
15	2.79 ± 1.06
16	62.1 ± 10.7
19	94.8 ± 1.50

Data are expressed as means ± standard deviation.

Table 3. *In Vivo* Biodistribution of [^{125}I]**3**

Tissues	2 min	30 min	1 h	3 h	6 h
Blood	7.4 ± 2.5	1.3 ± 0.5	1.0 ± 0.3	0.7 ± 0.3	0.5 ± 0.2
Stomach	0.7 ± 0.3	2.2 ± 2.1	1.0 ± 0.7	1.0 ± 0.9	0.7 ± 0.6
Intestine	3.6 ± 0.8	11.2 ± 3.0	16.5 ± 4.0	5.8 ± 3.1	5.3 ± 1.8
Kidney	68.1 ± 20.1	88.8 ± 26.5	92.8 ± 13.7	110 ± 44.6	97.1 ± 30.6
Liver	22.5 ± 4.7	13.7 ± 1.7	13.9 ± 3.1	9.0 ± 2.3	4.5 ± 1.3
Spleen	12.5 ± 5.3	43.3 ± 13.9	36.5 ± 13.9	16.1 ± 7.6	9.7 ± 7.3
Heart	5.4 ± 1.3	2.1 ± 0.9	1.3 ± 0.5	0.7 ± 0.4	0.4 ± 0.3
Lung	6.8 ± 1.8	2.9 ± 0.8	2.5 ± 0.5	1.2 ± 0.3	0.9 ± 0.3
Muscle	1.4 ± 0.2	0.6 ± 0.2	0.5 ± 0.2	0.2 ± 0.1	0.1 ± 0.0
LNCaP	4.2 ± 1.2	9.5 ± 5.9	7.0 ± 2.4	9.5 ± 3.1	6.7 ± 1.3
PC-3	2.7 ± 0.5	0.9 ± 0.3	0.7 ± 0.1	0.3 ± 0.1	0.2 ± 0.0
Thyroid	0.02 ± 0.01	0.00 ± 0.00	0.01 ± 0.00	0.01 ± 0.01	0.02 ± 0.00
LNCaP/PC-3	1.5	10.1	9.6	33.9	36.8
LNCaP/Blood	0.6	7.2	6.9	13.8	13.3
PC-3/Blood	0.4	0.7	0.7	0.4	0.4
LNCaP/Muscle	2.9	16.5	15.5	49.4	76.7

PC-3/Muscle	1.9	1.6	1.6	1.5	2.1

Accumulation in each tissue (except for stomach and thyroid, where it was evaluated as %ID) was evaluated as %ID/g. Values are expressed as means ± standard deviation. The ratios are based on the %ID/g.

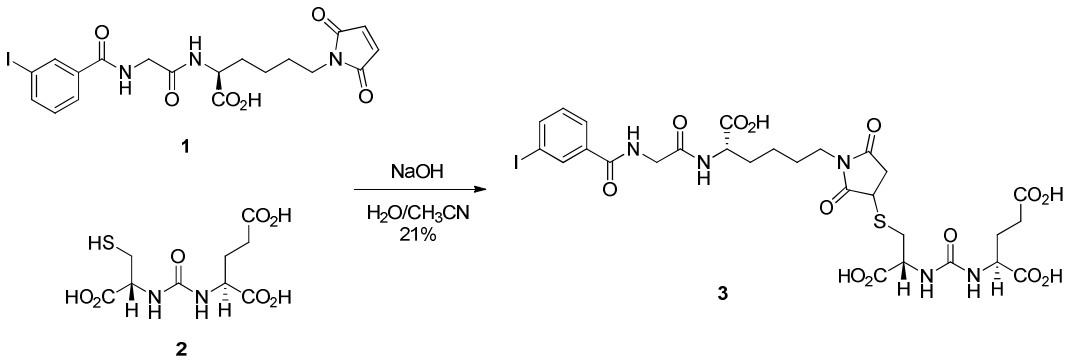

Scheme 1

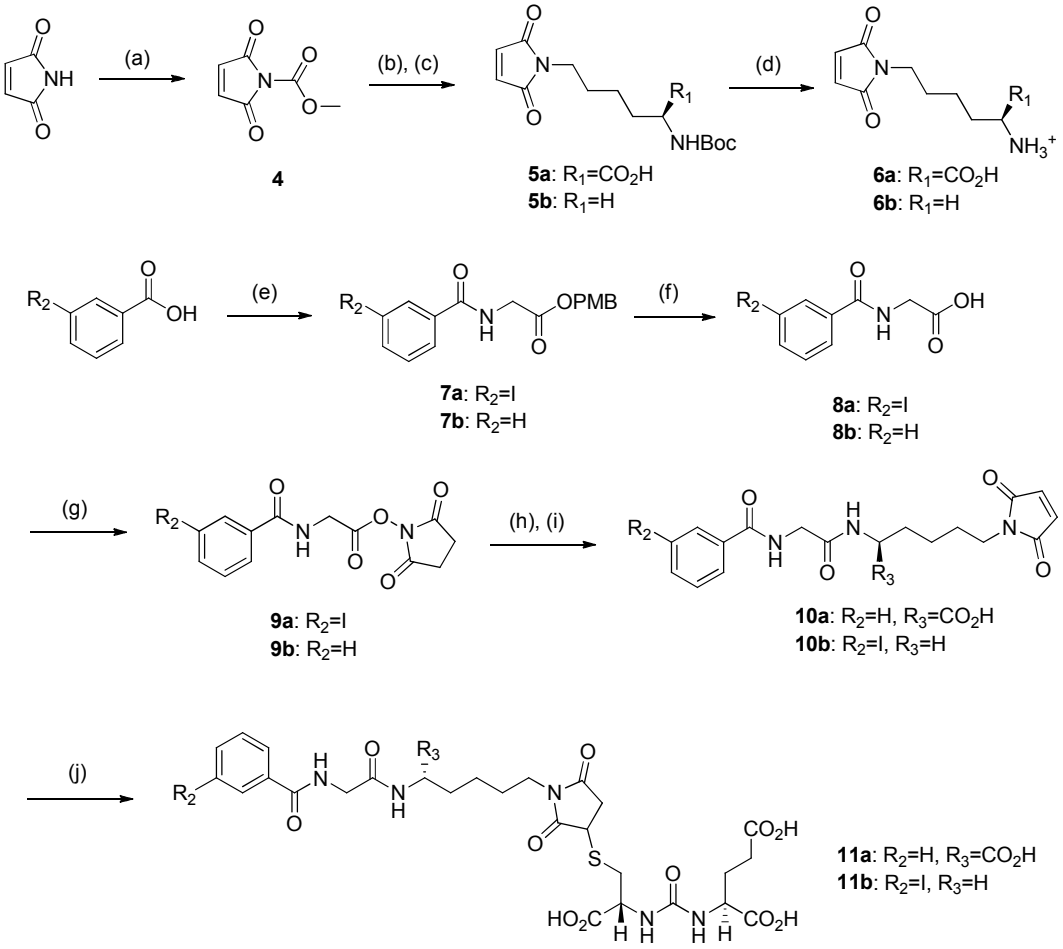

(a) *N*-Methylmorpholine, $ClCO_2CH_3$, ethyl acetate, 88%; (b) Boc-Lys-OH, $NaHCO_3$, H_2O, 76%; (c) $BocHNC_4H_8NH_2$, $NaHCO_3$, H_2O, 1,4-dioxane, 97%; (d) HCl, ethyl acetate, 66% (**6a**), 75% (**6b**); (e) H-Gly-OPMB, WSCI, Et_3N, DMF, 64% (**7a**), 57% (**7b**); (e) TFA, DCM, 97% (**8a**), 94% (**8b**); NHS, DIC, DMF, 62% (**9a**), 95% (**9b**); (h) **6a**, **9b**, DIPEA, CH_3CN, 32%; (i) **6b**, **9a**, DIPEA, CH_3CN, 46%; (j) **2**, NaOH, H_2O, CH_3CN, 54% (**11a**), 43% (**11b**).

Scheme 2

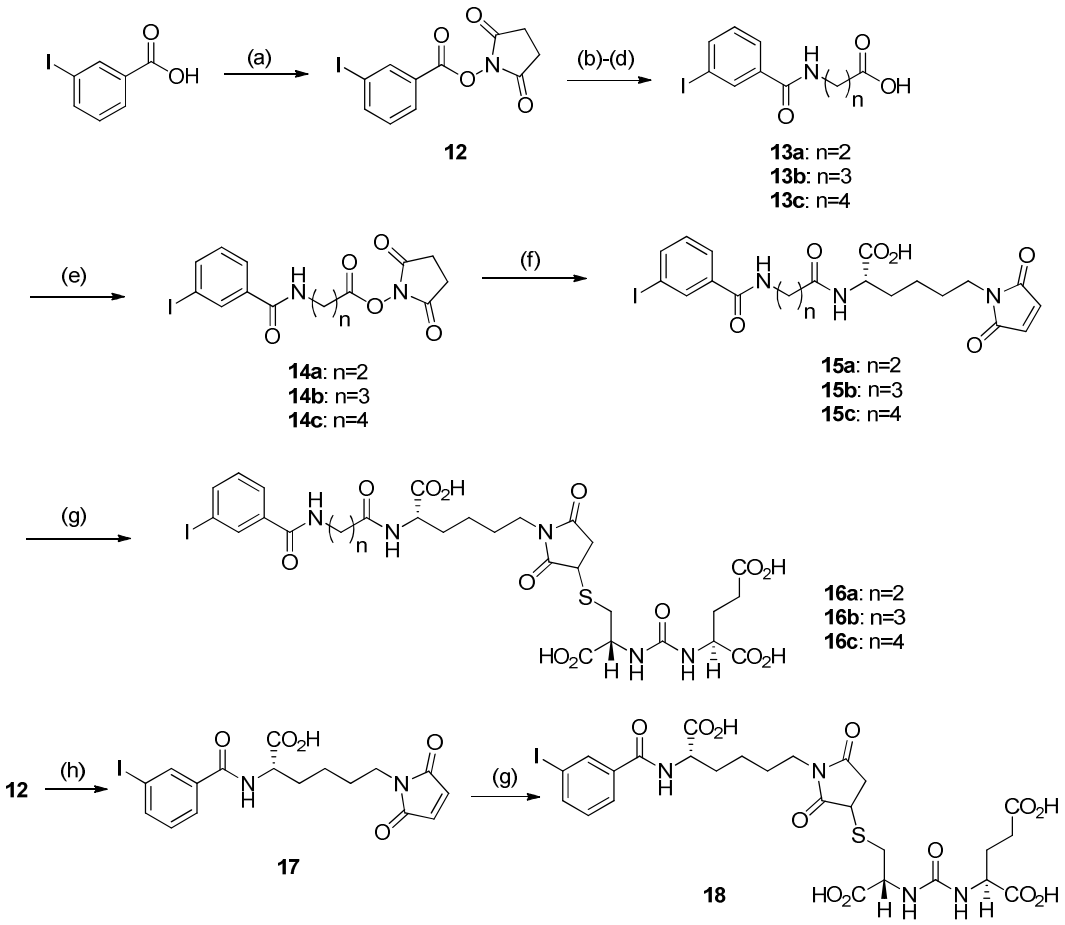

(a) DCC, NHS, 1,4-dioxane, 98%; (b) $H_2NC_3H_6COOH$, DIPEA, CH_3CN, 39%; (c) $H_2NC_4H_8COOH$, DIPEA, CH_3CN ,65%; (d) $H_2NC_5H_{10}COOH$, DIPEA, CH_3CN, 50%; (e) NHS, WSCI, DMF, 36% (**14a**), 60% (**14b**), 49% (**14c**); (f) **6a**, DIPEA, CH_3CN, 14% (**15a**), 17% (**15b**), 24% (**15c**); (g) **2**, NaOH, H_2O, CH_3CN, 58% (**16a**), 73% (**16b**), 23% (**16c**), 43% (**18**); (h) **6a**, DIPEA, CH_3CN, 26%.

Scheme 3

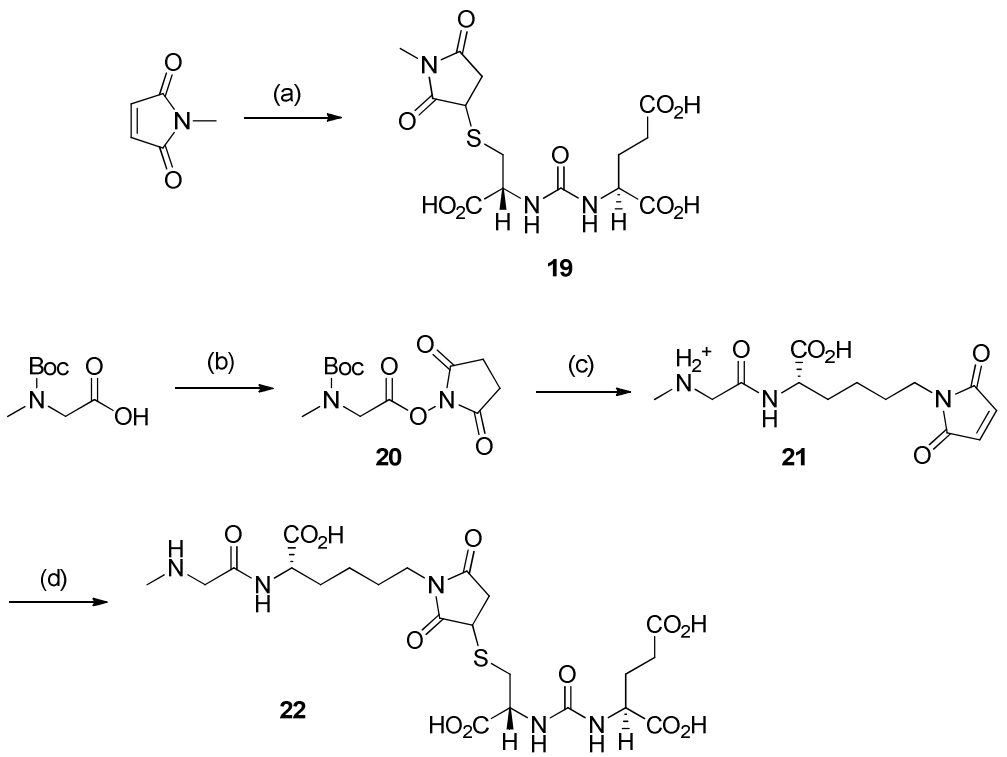

(a) **2**, NaOH, H_2O, CH_3CN, 45%; (b) *N*-hydroxysuccinimide, WSCI, DMF, 63%; (c) (i) **6a**, DIPEA, CH_3CN, (ii) HCl, ethyl acetate, 4% (2 steps); (d) **2**, NaOH, H_2O, 52%.

Scheme 4

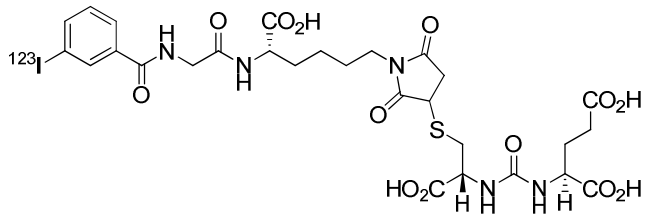

[^{123}I]IGLCE (**3**)

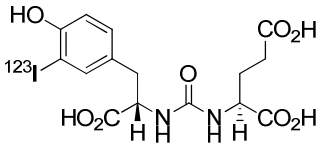

[^{123}I]DCIT (**23**)

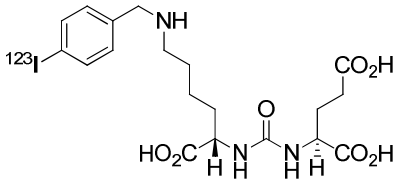

[^{123}I]MIP-1072 (**24**)

Figure 1

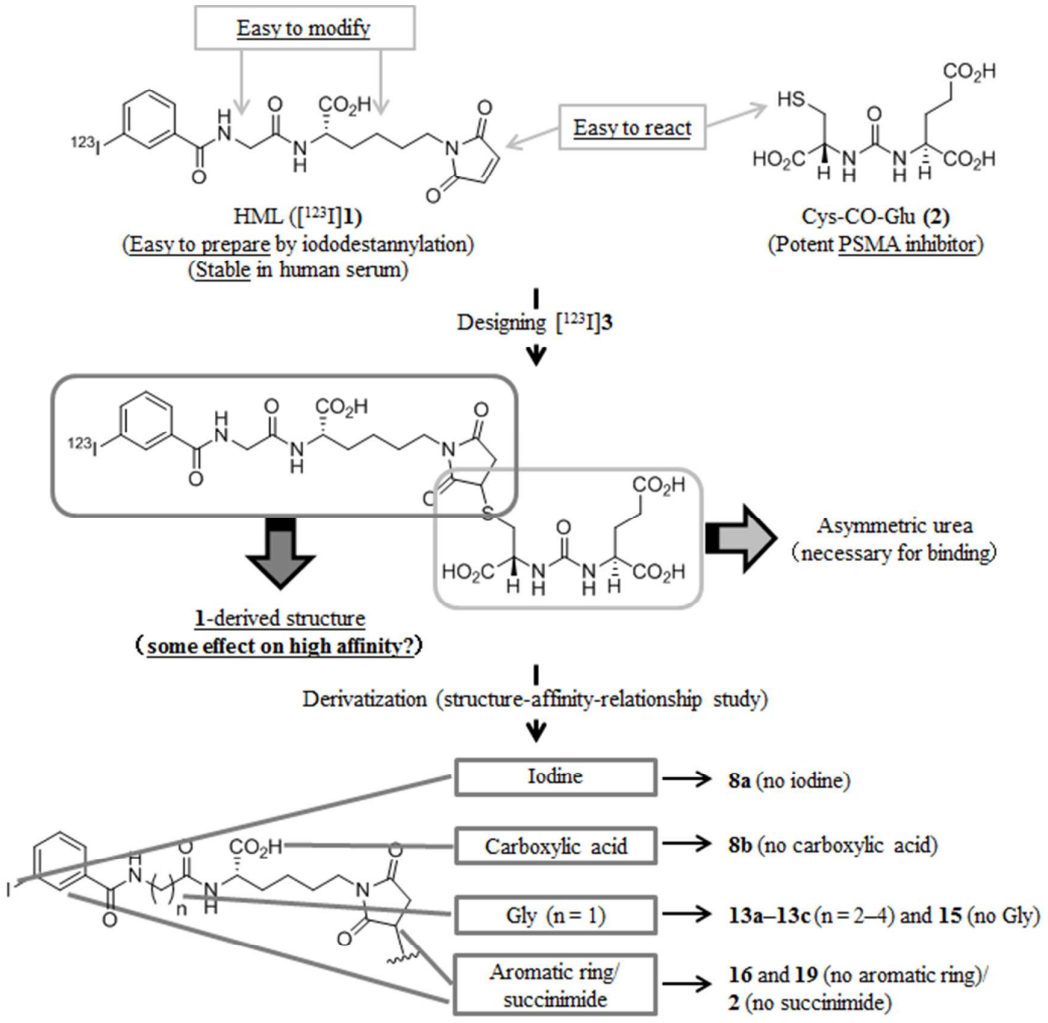
Easy to modify
Easy to react
HML ([123I]1)
(Easy to prepare by iododestannylation)
(Stable in human serum)
Cys-CO-Glu (2)
(Potent PSMA inhibitor)
Designing [123I]3
Asymmetric urea
(necessary for binding)
1-derived structure
(some effect on high affinity?)
Derivatization (structure-affinity-relationship study)
Iodine
8a (no iodine)
Carboxylic acid
8b (no carboxylic acid)
Gly (n = 1)
13a–13c (n = 2–4) and 15 (no Gly)
Aromatic ring/
succinimide
16 and 19 (no aromatic ring)/
2 (no succinimide)

Figure 2

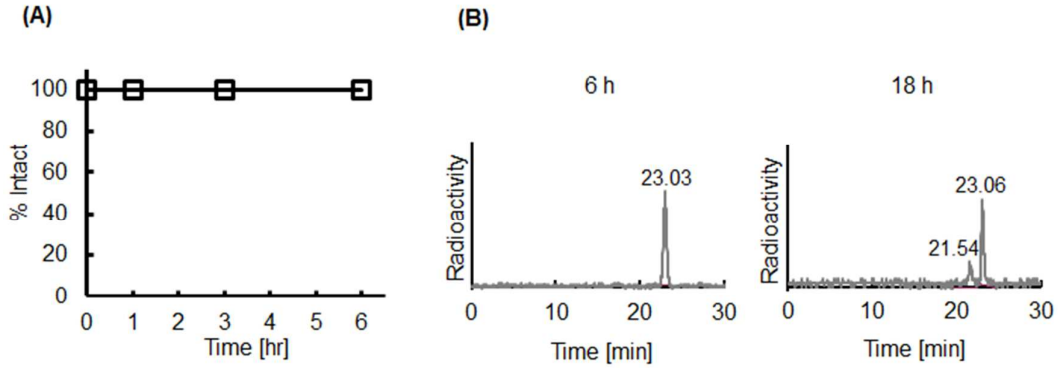
(A)
100
80
60
40
20
0
% Intact
0 1 2 3 4 5 6
Time [hr]
(B)
6 h
18 h
Radioactivity
23.03
23.06
21.54
0 10 20 30
Time [min]

Figure 3

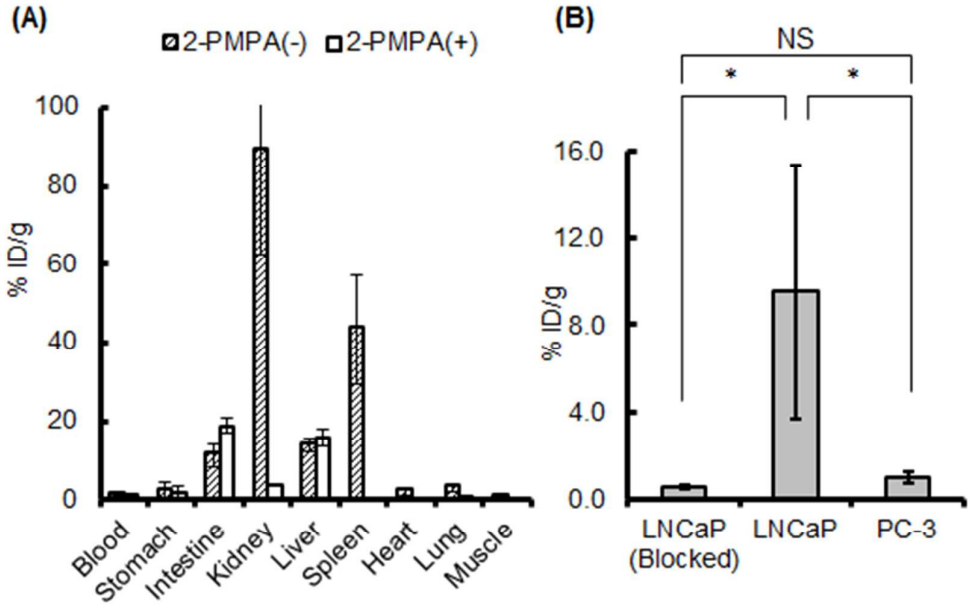
(A)
2-PMPA(-)
2-PMPA(+)
% ID/g
100
80
60
40
20
0
Blood
Stomach
Intestine
Kidney
Liver
Spleen
Heart
Lung
Muscle
(B)
NS
*
*
% ID/g
16.0
12.0
8.0
4.0
0.0
LNCaP (Blocked)
LNCaP
PC-3

Figure 4

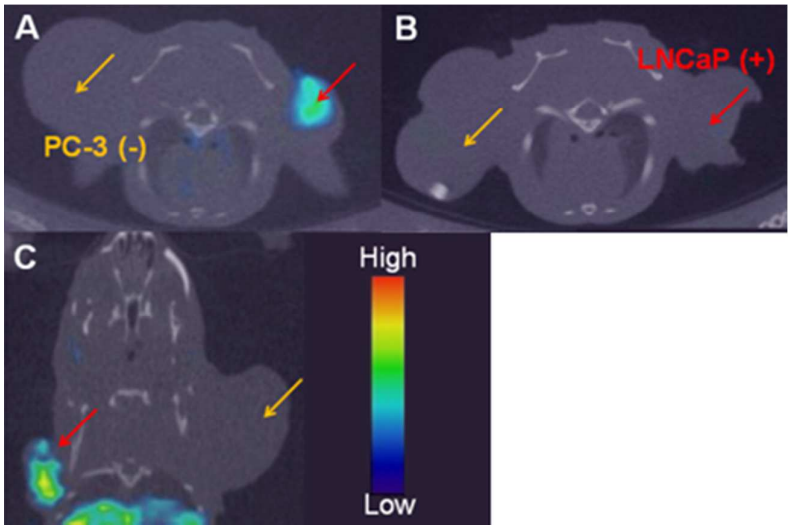

Figure 5

Scheme 1. Synthesis of IGLCE (**3**).

Scheme 2. Synthesis of type 1 and 2 derivatives.

Scheme 3. Synthesis of type 3 derivatives.

Scheme 4. Synthesis of type 4 derivatives.

Figure 1. Structures of ^{125}I-labeled probes used in this study.

Figure 2. Strategy for the design and derivatization of [^{123}I]**3**.

Figure 3. (A) Time-dependent degradation of [^{125}I]**3** over 6 h. No degradation products were observed over the 6 h incubation period. (B) Shown are radio-HPLC charts after 6 h (left) and 18 h incubations (right). The intact compound peaks elute at 23.03 min. The sub-peak at 21.5 min is likely 3-[^{125}I]iodohuppric acid.

Figure 4. In the blocking study, all mice were sacrificed 30 min after injection. Data for the

stomach are expressed as %ID. (A) In normal tissues, significant inhibition by 2-PMPA was observed in kidney and spleen. (B) Accumulation in LNCaP tumors was significantly inhibited by 2-PMPA. The difference between the accumulations in PC-3 tumors and blocked LNCaP tumors was not significant. (*$P < 0.05$, NS; not significant)

Figure 5. (A and B) Transaxial SPECT/CT images obtained with [^{123}I]**3**. Mice were injected with [^{123}I]**3** without (A) or with (B) 2-PMPA (50 mg/kg weight). [^{123}I]**3** clearly illuminated LNCaP tumors (A), and 2-PMPA prevented this reaction (B). [^{123}I]**3** did not accumulate in PC-3 tumors. (C) Coronal SPECT/CT images were obtained with [^{123}I]**3**.

Table of Contents Graphic